

On Robust Wasserstein Barycenter: The Model and Algorithm

Xu Wang* Jiawei Huang* Qingyuan Yang* Jinpeng Zhang*

Abstract

The *Wasserstein barycenter problem* is to compute the average of m given probability measures, which has been widely studied in many different areas; however, real-world data sets are often noisy and huge, which impedes its application in practice. Hence, in this paper, we focus on improving the computational efficiency of two types of *robust Wasserstein barycenter problem* (RWB): *fixed-support* RWB (fixed-RWB) and *free-support* RWB (free-RWB); actually, the former is a subroutine of the latter. Firstly, we improve efficiency through model reduction; we reduce RWB as an *augmented Wasserstein barycenter problem*, which works for both fixed-RWB and free-RWB. Especially, fixed-RWB can be computed within $\tilde{O}(\frac{mn^2}{\epsilon_+})$ time by using an off-the-shelf solver, where ϵ_+ is the pre-specified additive error and n is the size of locations of input measures. Then, for free-RWB, we leverage a quality guaranteed data compression technique, coresets, to accelerate computation by reducing the data set size m . It shows that running algorithms on the coresets is enough instead of on the original data set. Next, by combining the model reduction and coresets techniques above, we propose an algorithm for free-RWB by updating the weights and locations alternatively. Finally, our experiments demonstrate the efficiency of our techniques.

Keywords: Wasserstein barycenter, robust optimization, coresets.

1 Introduction

Wasserstein distance [38] is a popular metric for quantifying the difference between two probability distributions by the cost of mass transporting. *Wasserstein barycenter problem* [2] is to compute a measure ν that minimizes the sum of Wasserstein distances to the given m probability measures $\{\mu^1, \dots, \mu^m\}$. Wasserstein barycenter is a popular model for integrating multi-source information, where it can efficiently capture the geometric properties of the given data [34, 33].

However, real-world data sets can be noisy and contain outliers. The outliers can be located in space arbitrarily; thus, the solution of Wasserstein barycenter problem could be destroyed significantly even with a single outlier. To tackle its sensitivity to outliers, we focus on two types of *robust Wasserstein barycenter problem* (RWB)¹: *fixed-support* RWB (fixed-RWB) and *free-support* RWB (free-RWB). For the former, the locations of barycenter are pre-specified, so we only need to optimize the weights. For the latter, we usually solve it by updating the weights and locations alternatively.

Indeed, the outlier sensitivity is mainly due to its strict marginal constraints. Thus, to promote the robustness of the fixed-support Wasserstein barycenter, Le et al. [26] used a KL-divergence regularization term to alter the hard marginal constraints elegantly. Nevertheless, only for a particular case $m = 2$, this formulation can be solved efficiently in $\tilde{O}(mn^2/\epsilon_+)$ time, where ϵ_+ is the pre-specified additive error and n is the size of locations of input measures; moreover, it suffers from the numerical instability issues caused by the regularization term [32]. For the free-RWB, to our best knowledge, few work has been conducted on this.

Besides, the computational burden is also a big obstacle. The free-support Wasserstein barycenter is notoriously hard in computation [3], let alone its robust version. Usually, we can accelerate free-RWB by improving the computation at each iteration. Moreover, coresets [13], a popular data compression technique (defined in Definition 2.4), can also accelerate the computation by reducing the data set size m . Roughly speaking, a coresets is a small-size proxy of a large-scale input data set \mathcal{Q} with respect to some objective function while preserving the cost. Therefore, one can run an existing optimization algorithm on the coresets \mathcal{S} rather than on the whole data set \mathcal{Q} , and consequently the total complexity can be reduced.

*School of Computer Science and Technology, University of Science and Technology of China, worm,hjw0330,yangqingyuan,zjp123}@mail.ustc.edu.cn

¹Throughout this paper, the robustness refers to the outlier robustness.

Contributions: We improve the computational efficiency of both fixed-RWB and free-RWB. In our algorithm, the former is a subroutine of the latter (as shown in Algorithm 2). Our main contributions are as follows:

- Firstly, we consider model reduction. The method in Nietert et al. [31] can obtain the value of robust Wasserstein distance efficiently. But it does not compute the coupling (i.e., \mathbf{P} in Definition 2.2), which impedes its application in RWB. Thus, we reduce robust Wasserstein distance problem into an augmented *optimal transport* (OT) problem, which can be solved within $\tilde{\mathcal{O}}(\frac{n^2}{\epsilon_+})$ time by the off-the-shelf solver [22]. Moreover, our method can obtain both value and coupling efficiently. Based on this, we reduce RWB as an *augmented Wasserstein barycenter problem* (AWB); that is, free-RWB and fixed-RWB are reduced as *free-support* AWB (free-AWB) and *fixed-support* AWB (fixed-AWB) respectively. Especially, via this, fixed-RWB can be solved within $\tilde{\mathcal{O}}(\frac{mn^2}{\epsilon_+})$ time [12] (while Le et al. [26] can achieve this time complexity only for $m = 2$); moreover, the fixed-AWB is an *linear programming* (LP) problem, and thus bypasses the numerical instability issues. Besides, this is essentially a subroutine of free-RWB, thus helping to improve its computational efficiency at each iteration later.
- Then, for free-RWB, we accelerate computation by reducing the data set size m via coresets technique. We first introduce a method to obtain an $\mathcal{O}(1)$ -approximate solution $\tilde{\nu}$ (in Lemma 4.1). Then, we take $\tilde{\nu}$ as an anchor to construct an $\tilde{\mathcal{O}}(\min\{\text{ddim}, \frac{\log n/\epsilon}{\epsilon_+^2}\} \cdot \frac{n}{\epsilon_+^2})$ size coresets, and analyze its quality (in Theorem 4.1). Finally, we propose an algorithm for solving free-RWB by combining model reduction and coresets technique. More specifically, we use the coresets technique to accelerate the computation by reducing the data set size m . Meanwhile, to solve free-RWB, we can compute its corresponding free-AWB by updating the weights and locations alternatively; updating weights is computed by invoking fixed-AWB (as in Algorithm 2).

1.1 Other Related Works

Fixed-support Wasserstein barycenter: In recent years, a number of efficient algorithms have been proposed for computing approximation solution with additive error ϵ_+ for fixed-support Wasserstein barycenter.² For example, the Iterative Bregman projections (IBP) algorithm takes $\tilde{\mathcal{O}}(mn^2/\epsilon_+^2)$ time [4, 24]; the accelerated IBP needs $\tilde{\mathcal{O}}(mn^{5/2}/\epsilon_+)$ time [15]; the FastIBP requires $\tilde{\mathcal{O}}(mn^{7/3}/\epsilon_+^{4/3})$ time [27]. Especially, Dvinskikh and Tiapkin [12] achieved $\tilde{\mathcal{O}}(mn^2/\epsilon_+)$ time complexity by using area-convexity property and dual extrapolation techniques.

Coresets: As a popular data compression technique, coresets have been widely used in machine learning, such as clustering [8, 14, 5], regression [36] and robust optimization [18, 39]. Especially, some coresets methods have been proposed to reduce the data set size m . For instance, Ding et al. [10] presented a coresets method for geometric prototype problem; Cohen-Addad et al. [9] designed a coresets for power mean problem; both of them leverage the properties of metric, and can be used to accelerate existing Wasserstein barycenter algorithms. However, due to the fact that robust Wasserstein distance is not a metric, we need to develop new techniques for our free-RWB.

2 Preliminaries

Notations: We define $[n] := \{1, \dots, n\}$. We denote the ℓ_1 -norm of a vector by $\|\cdot\|_1$. Let $(\mathcal{X}, \text{dist})$ be a metric space. Let \mathbb{R}_+ be the non-negative real number set. We use $\mathcal{M}_+(\mathcal{X})$ to denote the positive measure space on \mathcal{X} , and $\mathcal{P}(\mathcal{X})$ the probability measure space.

We use capital boldface letters to denote matrices, such as \mathbf{C} ; C_{ij} is its element in the i -th row and j -th column. Similarly, vector is denoted by lowercase boldface letters, such as $\mathbf{a} := (a_1, \dots, a_d)^T \in \mathbb{R}^d$; a_i being its i -th element; $\mathbf{a} \succeq \mathbf{b}$ means $a_i \geq b_i$ for all $i \in [d]$. We define $(\mathbf{a}; \zeta) := (a_1, \dots, a_d, \zeta)^T$ for any $\zeta \in \mathbb{R}$. We use $\text{diag}(\mathbf{a})$ to denote a matrix with diagonal \mathbf{a} and 0 otherwise.

In the following, we will introduce several fundamental concepts.

DEFINITION 2.1. (WASSERSTEIN DISTANCE) Let $\mu = \sum_{i=1}^n a_i \delta_{x_i}, \nu = \sum_{j=1}^n b_j \delta_{y_j} \in \mathcal{P}(\mathcal{X})$ with $\mathbf{a}, \mathbf{b} \in \mathbb{R}_+^n$ being their weights respectively. Given a real number $z \geq 1$ and a cost matrix $\mathbf{C} \in \mathbb{R}_+^{n \times n}$ with $C_{ij} = \text{dist}^z(x_i, y_j)$, the z -th-Wasserstein distance between μ and ν is

²Let opt be the optimal value of fixed-support Wasserstein barycenter problem. The value induced by its approximation solution with additive error ϵ_+ is at most $\text{opt} + \epsilon_+$.

$$W_z(\mu, \nu) := \left(\min_{\mathbf{P} \in \Pi(\mathbf{a}, \mathbf{b})} \langle \mathbf{P}, \mathbf{C} \rangle \right)^{1/z},$$

where $\Pi(\mathbf{a}, \mathbf{b}) := \{\mathbf{P} \in \mathbb{R}_+^{n \times n} \mid \mathbf{P}\mathbf{1} = \mathbf{a}, \mathbf{P}^T\mathbf{1} = \mathbf{b}\}$ is the coupling set and $\mathbf{1}$ is the vector of ones.

The Wasserstein distance can capture geometrical structures well, and thus is a popular tool for measuring the similarity between two probability measures. However, due to its sensitivity to outliers, we introduce its robust version to mitigate the impact of outliers. The following robust Wasserstein distance [31] achieves the minimax optimal robust proxy for $W_p(\cdot, \cdot)$ under Huber contamination [20] model.

DEFINITION 2.2. (ROBUST WASSERSTEIN DISTANCE [31]) *Let $\mu, \nu, \mathbf{a}, \mathbf{b}, z, \mathbf{C}$ be the same as in Definition 2.1, and $\mu_{\text{out}}, \nu_{\text{out}} \in \mathcal{M}_+(\mathcal{X})$ be the measure of outliers for μ, ν respectively. Given $0 \leq \zeta_\mu, \zeta_\nu < 1$ and $\mathbf{a}_{\text{out}}, \mathbf{b}_{\text{out}}$ the weights of $\mu_{\text{out}}, \nu_{\text{out}}$, the robust Wasserstein distance $\mathcal{W}_z(\mu, \nu)$ between μ and ν can be solved by the following optimization problem*

$$(2.1) \quad \begin{aligned} \mathcal{W}_z^z(\mu, \nu) &:= \min_{\mathbf{a}_{\text{out}}, \mathbf{b}_{\text{out}}, \mathbf{P}} g(\mathbf{a}_{\text{out}}, \mathbf{b}_{\text{out}}, \mathbf{P}) \\ g(\mathbf{a}_{\text{out}}, \mathbf{b}_{\text{out}}, \mathbf{P}) &= \langle \mathbf{P}, \mathbf{C} \rangle \\ \text{s.t.}, \quad \mathbf{a} &\succeq \mathbf{a}_{\text{out}}, \|\mathbf{a}_{\text{out}}\|_1 = \zeta_\mu, \mathbf{b} \succeq \mathbf{b}_{\text{out}}, \|\mathbf{b}_{\text{out}}\|_1 = \zeta_\nu, \\ \mathbf{P} &\in \Pi \left(\frac{\mathbf{a} - \mathbf{a}_{\text{out}}}{1 - \zeta_\mu}, \frac{\mathbf{b} - \mathbf{b}_{\text{out}}}{1 - \zeta_\nu} \right). \end{aligned}$$

Note that we use different fonts to distinguish Wasserstein distance $W_z(\cdot, \cdot)$ and its robust version $\mathcal{W}_z(\cdot, \cdot)$. In Definition 2.2, μ, ν contain ζ_μ, ζ_ν masses of outliers, respectively. Moreover, $\|\frac{\mathbf{a} - \mathbf{a}_{\text{out}}}{1 - \zeta_\mu}\|_1 = 1$ and $\|\frac{\mathbf{b} - \mathbf{b}_{\text{out}}}{1 - \zeta_\nu}\|_1 = 1$ holds; therefore, $\frac{\mu - \mu_{\text{out}}}{1 - \zeta_\mu}, \frac{\nu - \nu_{\text{out}}}{1 - \zeta_\nu} \in \mathcal{P}(\mathcal{X})$ can be regarded as robust proxies of μ, ν .

Next, we introduce its corresponding two types of RWB: fixed-RWB and free-RWB. Now, we pre-specify some notations used throughout this paper. The input of fixed-RWB/free-RWB is a set of probability measures,

$$(2.2) \quad \mathcal{Q} := \left\{ \mu^l \mid \mu^l = \sum_{i=1}^n a_i^l \delta_{x_i^l} \right\}_{l \in [m]} \subseteq \mathcal{P}(\mathcal{X}),$$

where $\omega : \mathcal{Q} \rightarrow \mathbb{R}_+$ is the weight function of \mathcal{Q} . We also define $\omega_l := \omega(\mu^l)$. For simplicity, we consider the case that the locations of each measure in \mathcal{Q} are n points. $\mathcal{X}^l := \{x_i^l\}_{i \in [n]}$ and \mathbf{a}^l are the locations and weights of μ^l . We use $|\mathcal{Q}|$ to denote the number of measures in \mathcal{Q} . For any $\mathcal{Q}' \subseteq \mathcal{Q}$, we define $\omega(\mathcal{Q}') := \sum_{\mu \in \mathcal{Q}'} \omega(\mu)$. Let

$$(2.3) \quad \nu = \sum_{j=1}^n b_j \delta_{y_j}, \tilde{\nu} = \sum_{j=1}^n \tilde{b}_j \delta_{\tilde{y}_j} \in \mathcal{P}(\mathcal{X})$$

be two feasible solutions. $Y := \{y_j\}_{j \in [n]}$ and \mathbf{b} are the locations and weights of ν ; similarly, $\tilde{Y} := \{\tilde{y}_j\}_{j \in [n]}$ and $\tilde{\mathbf{b}}$ are the locations and weights of $\tilde{\nu}$.

DEFINITION 2.3. (RWB) *Given a set of probability measures \mathcal{Q} as in (2.2), the robust Wasserstein barycenter on \mathcal{Q} is a new probability measure $\nu^* \in \mathcal{P}(\mathcal{X})$ that minimizes the following objective*

$$(2.4) \quad \mathcal{WB}(\mathcal{Q}, \nu) := \frac{1}{\omega(\mathcal{Q})} \sum_{l=1}^m \omega_l \cdot \mathcal{W}_z^z(\mu^l, \nu) \quad \text{with } \nu \in \mathcal{P}(\mathcal{X}).$$

We call it fixed-RWB if the locations of ν are pre-specified; we call it free-RWB if the locations of ν can be optimized.

We define $\text{OPT} := \min_\nu \mathcal{WB}(\mathcal{Q}, \nu)$ as the optimal value induced by an optimal solution ν^* . A probability measure $\tilde{\nu} \in \mathcal{P}(\mathcal{X})$ is called an α -approximate solution if it achieves at most $\alpha \cdot \text{OPT}$.

Most optimization problems employ iterative algorithms; thus, the solution is generally limited to a local area after the initial rounds; for such scenarios, a local coresnet [39, 16] is enough.

DEFINITION 2.4. (LOCAL CORESET) Let \mathcal{Q} be the same as in (2.2) and $0 < \epsilon < 1$. We fix an anchor $\tilde{\nu}$ as in (2.3). The local ϵ -coreset \mathcal{S} is a subset of \mathcal{Q} with τ being its weight function and satisfies that, for all $\nu \in \mathcal{D}_{\tilde{\nu}}$,

$$(2.5) \quad |\mathcal{WB}(\mathcal{Q}, \nu) - \mathcal{WB}(\mathcal{S}, \nu)| \leq \epsilon \cdot \mathcal{WB}(\mathcal{Q}, \nu),$$

where we define $\mathcal{WB}(\mathcal{S}, \nu) := \frac{1}{\tau(\mathcal{S})} \sum_{\mu \in \mathcal{S}} \tau(\mu) \cdot \mathcal{W}_z^z(\mu, \nu)$ and $\mathcal{D}_{\tilde{\nu}} := \{\nu \in \mathcal{P}(\mathcal{X}) \mid W_z(\tilde{\nu}, \nu) \leq r\}$.

The ‘‘local’’ coreset means that (2.5) holds for all solutions in the local area $\mathcal{D}_{\tilde{\nu}}$. The local area $\mathcal{D}_{\tilde{\nu}}$ is anchored at the pre-specified solution $\tilde{\nu}$; specifically, the solution ν in $\mathcal{D}_{\tilde{\nu}}$ satisfies that the Wasserstein distance between $\nu, \tilde{\nu}$ is no larger than r .

Organization: The remainder of this paper is as follows. Section 3 focuses on model reduction for two types of RWB: free-RWB and fixed-RWB. Section 4 focuses on improving time efficiency for free-RWB; Sections 4.1 and 4.2 introduce coreset technique to reduce the data set size m and analyze its quality; Section 4.3 proposes an algorithm to solve free-RWB by combining model reduction and coreset technique.

3 Model Reduction

This section improves the computational efficiency from the perspective of model reduction. Section 3.1 reduces robust Wasserstein distance problem as augmented OT problem by Lemma 3.1; Section 3.2 reduces free-RWB as free-AWB in Theorem 3.1; Section 3.3 reduces fixed-RWB as fixed-AWB, which is essentially a special case of free-RWB.

3.1 Robust Wasserstein Distance To facilitate model reduction, we specify the following notations. Let $\mu, \nu, \mathbf{a}, \mathbf{b}, \zeta_\mu, \zeta_\nu, z$ be the same as in Definition 2.2 and \mathbf{o} the dummy point. Let $A \subseteq \{x_i\}_{i \in [n+1]}$ and $B \subseteq \{y_j\}_{j \in [n+1]}$ with $x_{n+1} = y_{n+1} = \mathbf{o}$. We define

$$(3.6) \quad \mu_{\text{aug}}(A) := \frac{\mu(A - \mathbf{o})}{1 - \zeta_\mu} + \mathbb{1}_{\mathbf{o} \in A} \cdot \frac{\zeta_\nu}{1 - \zeta_\nu}$$

$$\text{and its weights } \mathbf{a}_{\text{aug}} := \left(\frac{\mathbf{a}}{1 - \zeta_\mu}; \frac{\zeta_\nu}{1 - \zeta_\nu} \right)$$

$$(3.7) \quad \nu_{\text{aug}}(B) := \frac{\nu(B - \mathbf{o})}{1 - \zeta_\nu} + \mathbb{1}_{\mathbf{o} \in B} \cdot \frac{\zeta_\mu}{1 - \zeta_\mu}$$

$$\text{and its weights } \mathbf{b}_{\text{aug}} := \left(\frac{\mathbf{b}}{1 - \zeta_\nu}; \frac{\zeta_\mu}{1 - \zeta_\mu} \right),$$

where $\mathbb{1}_{\text{condition}}$ is 1 if the condition is true, and 0 otherwise.

PROBLEM 3.1. (AUGMENTED OT) For any real number $z \geq 1$, we define the augmented OT as the following optimization problem

$$(3.8) \quad \begin{aligned} \mathcal{AOT}(\mu_{\text{aug}}, \nu_{\text{aug}}) &:= \min_{\mathbf{P}_{\text{aug}} \in \Pi(\mathbf{a}_{\text{aug}}, \mathbf{b}_{\text{aug}})} h(\mathbf{P}_{\text{aug}}), \\ h(\mathbf{P}_{\text{aug}}) &:= \langle \mathbf{P}_{\text{aug}}, \mathbf{C}_{\text{aug}} \rangle \quad \text{s.t.}, \quad (P_{\text{aug}})_{n+1, n+1} = 0, \end{aligned}$$

where $(C_{\text{aug}})_{ij} := \mathbb{1}_{i \in [n] \text{ and } j \in [n]} \cdot \text{dist}^z(x_i, y_j)$.

REMARK 3.2. We use a similar dummy point idea as in [7, 11]. $(P_{\text{aug}})_{n+1, n+1} = 0$ always holds for the optimal solution of $h(\cdot)$ in (3.8). We write it explicitly to facilitate the construction of a bijection φ later; via φ , we can regard (2.1) and (3.8) as equivalence.

Actually, OT is a generalization of Wasserstein distance. The cost function of Wasserstein distance must be induced by a metric, while OT only requires the cost function to be a non-negative real value function. Therefore, Problem 3.1 is indeed an OT problem.

Next, we illustrate that (2.1) is equivalent to (3.8) under a map φ . Let \mathcal{D}_g and \mathcal{D}_h be the feasible domain of (2.1) and (3.8) respectively. We construct a map φ from \mathcal{D}_g to \mathcal{D}_h as follows,

$$(3.9) \quad \varphi : \mathcal{D}_g \rightarrow \mathcal{D}_h, (\mathbf{a}_{\text{out}}, \mathbf{b}_{\text{out}}, \mathbf{P}) \mapsto \mathbf{P}_{\text{aug}},$$

where $(P_{\text{aug}})_{ij} = \mathbb{1}_{i \in [n] \text{ and } j \in [n]} \cdot P_{ij} + \mathbb{1}_{i \in [n] \text{ and } j = n+1} \cdot \frac{(a_{\text{out}})_i}{1-\zeta_\mu} + \mathbb{1}_{i = n+1 \text{ and } j \in [n]} \cdot \frac{(b_{\text{out}})_j}{1-\zeta_\nu}$.

LEMMA 3.1. (2.1) is equivalent to (3.8) under bijection φ ; that is, $h = g\varphi^{-1}$ and $h\varphi = g$. More specifically, for any $\mathbf{P}_{\text{aug}} \in \mathcal{D}_h$, $h(\mathbf{P}_{\text{aug}}) = g\varphi^{-1}(\mathbf{P}_{\text{aug}})$ holds; for any $(\mathbf{a}_{\text{out}}, \mathbf{b}_{\text{out}}, \mathbf{P}) \in \mathcal{D}_g$, $h\varphi(\mathbf{a}_{\text{out}}, \mathbf{b}_{\text{out}}, \mathbf{P}) = g(\mathbf{a}_{\text{out}}, \mathbf{b}_{\text{out}}, \mathbf{P})$ holds.

The proof of Lemma 3.1 is deferred to Appendix.

REMARK 3.3. Removing the last condition in (3.8) does not affect the result; thus, it is a classic OT problem. Nietert et al. [31] computed the value of robust Wasserstein distance efficiently by its dual problem; however, it does not offer coupling, which impedes its applications to RWB. Our method can obtain coupling within $\tilde{\mathcal{O}}(\frac{n^2}{\epsilon_+})$ time efficiently [22], which makes it possible to apply this technique to solve RWB.

3.2 Free-support Robust Wasserstein Barycenter This section reduces free-RWB as free-AWB. **Note that**, henceforth, we consider the case that, for $\mathcal{W}_z(\cdot, \cdot)$ and $\mathcal{WB}(\cdot, \cdot)$, the measure of the first parameter contains ζ mass of outliers; and the measure of the second parameter contains no outliers.

PROBLEM 3.4. (free-AWB) The free-support augmented Wasserstein barycenter on \mathcal{Q} is a new probability measure $\nu^* \in \mathcal{P}(\mathcal{X})$ that minimizes the following objective

$$(3.10) \quad \text{AWB}(\mathcal{Q}, \nu) := \frac{1}{\omega(\mathcal{Q})} \sum_{l=1}^m \omega_l \cdot \text{AOT}(\mu_{\text{aug}}^l, \nu_{\text{aug}})$$

for $\nu \in \mathcal{P}(\mathcal{X})$, where $\mu_{\text{aug}}^l(A) = \frac{\mu^l(A - \mathfrak{o})}{1-\zeta}$ for $\mu^l \in \mathcal{Q}$ and $\nu_{\text{aug}}(B) := \nu(B - \mathfrak{o}) + \mathbb{1}_{\mathfrak{o} \in B} \cdot \frac{\zeta}{1-\zeta}$.

Also, the first parameter of both $\mathcal{WB}(\cdot, \cdot)$, $\text{AWB}(\cdot, \cdot)$ is an input measure set, and the second parameter is called feasible solution.

THEOREM 3.1. For any feasible solution $\nu \in \mathcal{P}(\mathcal{X})$, (2.4) and (3.10) induce the same cost; more specifically, $\mathcal{WB}(\mathcal{Q}, \nu) = \text{AWB}(\mathcal{Q}, \nu)$ for all $\nu \in \mathcal{P}(\mathcal{X})$.

The proof of Theorem 3.1 is in Appendix.

By Theorem 3.1, we can solve free-RWB by computing free-AWB. Moreover, it can be extended to the case that barycenter contains ζ_ν mass of outliers and μ^l contains ζ_μ mass of outliers. Besides, both Lemma 3.1 and Theorem 3.1 work for arbitrary probability measures, such as continuous, semi-continuous, discrete measures [32].

3.3 Fixed-support Robust Wasserstein Barycenter Actually, fixed-RWB/ fixed-AWB is a special case of free-RWB/free-AWB by pre-specifying the locations of barycenter. We fix the locations Y of ν as in (2.3). Then, the fixed-RWB on \mathcal{Q} is to find a measure $\nu \in \mathcal{P}(\mathcal{X})$ located on Y that minimizes

$$(3.11) \quad \begin{aligned} \mathcal{WB}_Y(\mathcal{Q}, \nu) &:= \frac{1}{\omega(\mathcal{Q})} \sum_{l=1}^m \omega_l \cdot \langle \mathbf{P}^l, \mathbf{C}^l \rangle \\ \text{s.t. } \mathbf{P}^l &\in \mathbb{R}_+^{n \times n}, \mathbf{1}^T \mathbf{P}^l \mathbf{1} = 1, \mathbf{P}^l \mathbf{1} \preceq \frac{\mathbf{a}^l}{1-\zeta} \text{ for } l \in [m] \\ (\mathbf{P}^l)^T \mathbf{1} &= (\mathbf{P}^{l+1})^T \mathbf{1} \text{ for } l \in [m-1], \end{aligned}$$

where $\mathbf{C}^l \in \mathbb{R}_+^{n \times n}$ is the cost matrix between μ^l and ν with $C_{ij}^l = \text{dist}^z(x_i^l, y_j)$.

By using Theorem 3.1, the fixed-RWB is equivalent to the following fixed-AWB

$$(3.12) \quad \begin{aligned} \text{AWB}_Y(\mathcal{Q}, \nu) &:= \frac{1}{\omega(\mathcal{Q})} \sum_{l=1}^m \omega_l \langle \mathbf{P}_{\text{aug}}^l, \mathbf{C}_{\text{aug}}^l \rangle \\ \text{s.t. } \mathbf{P}_{\text{aug}}^l &\in \Pi(\mathbf{a}_{\text{aug}}^l, \mathbf{b}_{\text{aug}}), \quad (\mathbf{b}_{\text{aug}})_{n+1} = \frac{\zeta}{1-\zeta}, \end{aligned}$$

where $\mathbf{C}_{\text{aug}}^l \in \mathbb{R}_+^{n \times (n+1)}$ is the cost matrix between μ_{aug}^l and ν_{aug} with $(\mathbf{C}_{\text{aug}}^l)_{ij} = \mathbb{1}_{i \in [n]} \text{ and } j \in [n] \cdot \text{dist}^z(x_i^l, y_j)$.

REMARK 3.5. For fixed-RWB, the locations of ν are pre-specified; thus, $\mathbf{C}_{\text{aug}}^l$ is constant. Obviously, fixed-RWB is a linear programming (LP) problem, which can be solved within $\tilde{\mathcal{O}}(\frac{mn^2}{\epsilon_+})$ time [12]. Other algorithms for fixed-support Wasserstein barycenter in Section 1.1 can also be used to solve fixed-RWB.

REMARK 3.6. Our fixed-RWB has the following advantages: (i) The method in [26] can achieve $\tilde{\mathcal{O}}(\frac{mn^2}{\epsilon_+})$ time complexity only for $m = 2$; however, our method can achieve it for all $m \geq 2$. (ii) The method [26] achieves robustness by adding an elegant KL-divergence regularization term to its objective; however, this term makes it suffer from numerical instability [32]; while our fixed-RWB is an LP essentially, and thus bypasses this problem.

4 Algorithm for Free-support Robust Wasserstein Barycenter

This section focuses on improving the computational efficiency of free-RWB. Section 4.1 constructs a local coresets and Section 4.2 analyzes its quality. Section 4.3 proposes an algorithm for solving free-RWB, which leverages coresets technique and model reduction.

4.1 Algorithm for Constructing Coresets This section uses coresets technique to reduce the data set size m for free-RWB. Now, we provide a method to obtain an approximate solution for free-RWB, which is an appropriate ‘‘anchor’’ for constructing a local coresets later.

LEMMA 4.1. Let $\alpha > 1$. If we select t measures $\{\mu^{q^1}, \dots, \mu^{q^t}\}$ from \mathcal{Q} according to the distribution $\frac{\omega_l}{\omega(\mathcal{Q})}$. Let X^{q^i} be the locations of μ^{q^i} and

$$\tilde{\nu} = \arg \min_{\nu} \{ \mathcal{WB}_X(\mathcal{Q}, \nu) \mid X \in \{X^{q^1}, \dots, X^{q^t}\} \}.$$

Then, $\tilde{\nu}$ yields a $2^z \alpha$ -approximate solution for free-RWB on \mathcal{Q} with probability at least $1 - \alpha^{-t}$. If $\alpha = \mathcal{O}(1)$, we can obtain an $\mathcal{O}(1)$ -approximate solution.

The proof of Lemma 4.1 is deferred to Appendix.

Coresets construction: Let \mathcal{Q} be the same as in (2.2) and $K = \lceil \log \frac{1}{\epsilon} \rceil$. Let $\tilde{\nu} = \sum_{j=1}^n \tilde{b}_j \delta_{\tilde{y}_j} \in \mathcal{P}(\mathcal{X})$ be an $\mathcal{O}(1)$ -approximate solution of free-RWB on \mathcal{Q} and $H = \sqrt[3]{\mathcal{WB}(\mathcal{Q}, \tilde{\nu})}$. Then, by using anchor $\tilde{\nu}$, we partition \mathcal{Q} into $K + 2$ layers³, i.e., $\mathcal{Q} = \sqcup_{k=0}^{K+1} \mathcal{Q}_k$,

$$(4.13) \quad \begin{aligned} \mathcal{Q}_0 &= \{ \mu \in \mathcal{Q} \mid \mathcal{W}_z(\mu, \tilde{\nu}) \leq H \} \\ \mathcal{Q}_k &= \{ \mu \in \mathcal{Q} \mid 2^{k-1}H < \mathcal{W}_z(\mu, \tilde{\nu}) \leq 2^k H \} \text{ for } k \in [K] \\ \mathcal{Q}_{K+1} &= \{ \mu \in \mathcal{Q} \mid \mathcal{W}_z(\mu, \tilde{\nu}) > 2^K H \}. \end{aligned}$$

Then, for any \mathcal{Q}_k with $0 \leq k \leq K$, if $|\mathcal{Q}_k| \leq \Gamma$, we take \mathcal{Q}_k as \mathcal{S}_k , and keep their original weights constant; if $|\mathcal{Q}_k| > \Gamma$, we take Γ samples \mathcal{S}_k from \mathcal{Q}_k according to distribution $\mathbb{1}_{\mu^l \in \mathcal{Q}_k} \cdot \frac{\omega_l}{\omega(\mathcal{Q}_k)}$, and set $\tau(\mu) = \frac{\omega(\mathcal{Q}_k)}{\Gamma}$ for $\mu \in \mathcal{S}_k$.

Intuitively, the measure μ in the outermost layer \mathcal{Q}_{K+1} is too far from the local area $\mathcal{D}_{\tilde{\nu}}$. For a fixed $\mu \in \mathcal{Q}_{K+1}$, the costs $\mathcal{W}_z(\mu, \nu)$ induced by all solutions in $\mathcal{D}_{\tilde{\nu}}$ are similar; thus, we can sample less points. For the outermost layer \mathcal{Q}_{K+1} , we set $\mathcal{S}_{K+1} = \{\mu^{\max}, \mu^{\min}\}$, where

$$(4.14) \quad \begin{aligned} \mu^{\max} &:= \arg \max_{\mu \in \mathcal{Q}_{K+1}} \mathcal{W}_z(\mu, \tilde{\nu}) \\ \mu^{\min} &:= \arg \min_{\mu \in \mathcal{Q}_{K+1}} \mathcal{W}_z(\mu, \tilde{\nu}). \end{aligned}$$

³The notation \sqcup denotes disjoint union of sets.

We set their weight as $\tau(\mu^{\max})$ and $\tau(\mu^{\min})$ satisfying

$$(4.15) \quad \begin{aligned} & \tau(\mu^{\max}) \cdot \mathcal{W}_z^z(\mu^{\max}, \tilde{\nu}) + \tau(\mu^{\min}) \cdot \mathcal{W}_z^z(\mu^{\min}, \tilde{\nu}) \\ &= \sum_{\mu \in \mathcal{Q}_{K+1}} \omega(\mu) \cdot \mathcal{W}_z^z(\mu, \tilde{\nu}). \end{aligned}$$

Then, we put all \mathcal{S}_k together to obtain \mathcal{S} . The details for constructing coresets are shown in Algorithm 1.

Algorithm 1 Coreset for free-RWB

Input: Probability measure set \mathcal{Q} ,

$\mathcal{O}(1)$ -approximate solution $\tilde{\nu}$.

- 1: Let $K = \lceil \log \frac{1}{\epsilon} \rceil$ and $H = \sqrt[z]{\mathcal{WB}(\mathcal{Q}, \tilde{\nu})}$;
- 2: Partition \mathcal{Q} into $K + 2$ layers $\{\mathcal{Q}_0, \mathcal{Q}_1, \dots, \mathcal{Q}_{K+1}\}$ as in (4.13);
- 3: **for** each \mathcal{Q}_k with $0 \leq k \leq K$ **do**
- 4: **if** $|\mathcal{Q}_k| \leq \Gamma$ **then**
- 5: $\triangleright \Gamma$ will be specified in Theorem 4.1;
- 6: Set $\mathcal{S}_k = \mathcal{Q}_k$ and set $\tau(\mu) = \omega(\mu)$ for $\mu \in \mathcal{Q}_k$;
- 7: **else**
- 8: Take samples \mathcal{S}_k with $|\mathcal{S}_k| = \Gamma$ according to the distribution $\mathbb{1}_{\mu' \in \mathcal{Q}_k} \cdot \frac{\omega_{\Gamma}}{\omega(\mathcal{Q}_k)}$, and set $\tau(\mu) = \frac{\omega(\mathcal{Q}_k)}{\Gamma}$ for $\mu \in \mathcal{S}_k$;
- 9: **end if**
- 10: **end for**
- 11: We set $\mathcal{S}_{K+1} = \{\mu^{\min}, \mu^{\max}\}$, and set their weights as in (4.14) and (4.15);
- 12: $\mathcal{S} = \cup_{k=0}^{K+1} \mathcal{S}_k$;

Output: the coreset \mathcal{S} for \mathcal{Q} .

REMARK 4.1. Our coreset method is inspired by the layered sampling in [8, 5], which is analyzed on metric space. However, our robust Wasserstein distance is not a metric, and thus new techniques are needed to analyze it.

4.2 Theoretical Analysis In this section, we prove the quality guarantee of our Algorithm 1 in Theorem 4.1.

THEOREM 4.1. We set $r = H$ in Definition 2.4. Suppose the diameter of \mathcal{X} is R , i.e., $\max_{x, y \in \mathcal{X}} \text{dist}(x, y) = R$ and the metric space has doubling dimension ddim . Let $\tilde{\nu}$ be an $\mathcal{O}(1)$ -approximate solution of free-RWB on \mathcal{Q} and $\Gamma = \tilde{\mathcal{O}}(\min\{\text{ddim}, \frac{\log n/\epsilon}{\epsilon^2}\} \cdot \frac{n}{\epsilon^2})$. With probability at least $1 - \eta$, Algorithm 1 outputs a local coreset \mathcal{S} for free-RWB on \mathcal{Q} .

REMARK 4.2. (i) The doubling dimension⁴ is a measure for describing the growth rate of the data set \mathcal{X} with respect to the metric $\text{dist}(\cdot, \cdot)$; (ii) The coreset size in Theorem 4.1 is dependent of the dataset set size m ; (iii) If ν is an α -approximate solution on \mathcal{S} , then it is also a $\frac{1+\epsilon}{1-\epsilon}\alpha$ -approximate solution on \mathcal{Q} with probability at least $1 - \eta$; thus, the approximate solution on \mathcal{S} can imitate the approximate solution on \mathcal{Q} well.

From the iterative size reduction [30] and the terminal version of Johnson-Lindenstrauss Lemma [6], we can regard $\text{ddim} = \tilde{\mathcal{O}}(\frac{\log n/\epsilon}{\epsilon^2})$. Therefore, it is sufficient to obtain a coreset with size $\tilde{\mathcal{O}}(\frac{n \cdot \text{ddim}}{\epsilon^2})$.

LEMMA 4.2. Given $r, \tilde{\nu}, \mathcal{D}_{\tilde{\nu}}$ as in Definition 2.4 and $0 < s \leq 1$, we have $\mathcal{W}_z^z(\mu, \nu) \leq (1 + s)^{z-1} \cdot \mathcal{W}_z^z(\mu, \tilde{\nu}) + (1 + \frac{1}{s})^{z-1} \cdot r^z$ for any $\mu \in \mathcal{Q}, \nu \in \mathcal{D}_{\tilde{\nu}}$.

Lemma 4.2 indicates that, for any fixed μ , the robust Wasserstein distance between μ and all the solutions in $\mathcal{D}_{\tilde{\nu}}$ can be bounded. Based on this, we can obtain the following lemma. (The proofs of Lemma 4.2 and Lemma 4.3 are in Appendix.)

⁴The doubling dimension is defined in Appendix.

LEMMA 4.3. We set $r = H$ in Definition 2.4. Let $\tilde{\nu}$ be an $\mathcal{O}(1)$ -approximate solution of free-RWB on \mathcal{Q} . For a fixed solution $\nu \in \mathcal{D}_{\tilde{\nu}}$, if we set $\Gamma = \mathcal{O}(\frac{\log 1/\eta}{\epsilon^2})$ in Algorithm 1, with probability at least $1 - \eta$, we have

$$|\mathcal{WB}(\mathcal{Q}, \nu) - \mathcal{WB}(\mathcal{S}, \nu)| \leq \mathcal{O}(\epsilon) \cdot \mathcal{WB}(\mathcal{Q}, \nu).$$

However, Lemma 4.3 only works for a single solution $\nu \in \mathcal{D}_{\tilde{\nu}}$. To ensure (2.5) holds for all the solutions in $\mathcal{D}_{\tilde{\nu}}$, we take two steps: (i) discrete the solution space $\mathcal{D}_{\tilde{\nu}}$ by grid \mathcal{F} (defined in (4.16)), and make sure it holds for all solutions in \mathcal{F} ; (ii) bound the discretization error and make sure it holds for all $\nu \in \mathcal{D}_{\tilde{\nu}}$. (The above two steps are exactly the roadmap for proving Theorem 4.1.)

Proof. Discrete the solution space $\mathcal{D}_{\tilde{\nu}}$: Suppose R is the diameter of \mathcal{X} . We define $\mathbb{B}(x, R) := \{y \mid \text{dist}(x, y) \leq R\}$.

Let $\mathbb{B}_j^{\epsilon H}$ be an ϵH -net of the ball $\mathbb{B}(\tilde{y}_j, R)$. Since the metric space $(\mathcal{X}, \text{dist})$ has doubling dimension ddim , we have $|\mathbb{B}_j^{\epsilon H}| = (\frac{R}{\epsilon H})^{\mathcal{O}(\text{ddim})}$. Let $e = \lceil \frac{nR^z}{\epsilon^z H^z} \rceil$ and $E = \{\frac{i}{e} \mid i \in [e]\}$ be a $\frac{\epsilon^z H^z}{nR^z}$ -net of the interval $[0, 1]$. Then, we consider a grid \mathcal{F} as follows.

$$(4.16) \quad \mathcal{F} := \left\{ \bar{\nu} = \sum_{j=1}^n \bar{b}_j \delta_{\bar{y}_j} \in \mathcal{P}(\mathcal{X}) \mid \bar{b}_j \in E, \bar{y}_j \in \mathbb{B}_j^{\epsilon H} \right\}$$

Thus, we obtain $|\mathcal{F}| \leq (\frac{R}{\epsilon H})^{\mathcal{O}(n \cdot \text{ddim})} \cdot (\frac{nR}{\epsilon H})^{\mathcal{O}(n)}$. By using union bound for $|\mathcal{F}|$ solutions, it yields that (2.5) holds for all the solutions in \mathcal{F} with probability at least $1 - \eta$ if we set $\Gamma = \mathcal{O}(\frac{n \log 1/\eta}{\epsilon^2} (\text{ddim} \cdot \log \frac{R}{\epsilon H} + \log n))$.

Bound discretization error: For any $\nu = \sum_{j=1}^n b_j \delta_{y_j} \in \mathcal{D}_{\tilde{\nu}}$, we can find a $\bar{\nu}' = \sum_{j=1}^n b_j \delta_{\bar{y}_j}$ satisfying $\text{dist}(y_j, \bar{y}_j) \leq \mathcal{O}(\epsilon H)$. For $W_z(\nu, \bar{\nu}')$, we can construct a feasible coupling by assigning all the mass of y_j to \bar{y}_j for all $j \in [n]$; that is, the coupling is a diagonal matrix $\text{diag}(\mathbf{b})$. Then, the cost induced by the feasible coupling $\text{diag}(\mathbf{b})$ is at most $\mathcal{O}(\epsilon^z H^z)$. Since $W_z^z(\nu, \bar{\nu}')$ is induced by the optimal coupling, we have $W_z^z(\nu, \bar{\nu}') \leq \mathcal{O}(\epsilon^z H^z)$.

Meanwhile, for $\bar{\nu}'$, we can find a $\bar{\nu} = \sum_{j=1}^n \bar{b}_j \delta_{\bar{y}_j} \in \mathcal{F}$ satisfying $b_j - \bar{b}_j \leq \frac{\epsilon^z H^z}{nR^z}$. For $W_z(\bar{\nu}, \bar{\nu}')$, we can construct a feasible coupling by keeping $b_j - \frac{|b_j \cdot e|}{e}$ mass constant; thus, we need to assign at most $\mathcal{O}(\frac{\epsilon^z H^z}{R^z})$ mass in total; obviously, the cost caused by this feasible coupling is at most $\mathcal{O}(\frac{\epsilon^z H^z}{R^z}) \cdot R^z$. Therefore, we have $W_z^z(\bar{\nu}, \bar{\nu}') \leq \epsilon^z H^z$. Finally, for any $\nu \in \mathcal{D}_{\tilde{\nu}}$, we can find a grid point $\bar{\nu}$ satisfying $W_z^z(\bar{\nu}, \nu) \leq \mathcal{O}(\epsilon^z) \cdot H^z$.

Similar to Lemma 4.2, we have $W_z^z(\mu, \nu) \leq (1 + \epsilon)^{z-1} \cdot W_z^z(\mu, \bar{\nu}) + (1 + \frac{1}{\epsilon})^{z-1} \cdot W_z^z(\nu, \bar{\nu})$ and $W_z^z(\mu, \nu) \geq (1 - \mathcal{O}(\epsilon)) \cdot W_z^z(\mu, \bar{\nu}) - \mathcal{O}(\frac{1}{\epsilon})^{z-1} \cdot W_z^z(\nu, \bar{\nu})$. Then,

$$\begin{aligned} & |\mathcal{WB}(\mathcal{Q}, \nu) - \mathcal{WB}(\mathcal{S}, \nu)| \\ &= \frac{1}{\omega(\mathcal{Q})} \left| \sum_{\mu \in \mathcal{Q}} \omega(\mu) \cdot W_z^z(\mu, \nu) - \sum_{\mu \in \mathcal{S}} \tau(\mu) \cdot W_z^z(\mu, \nu) \right| \\ &\leq \frac{1}{\omega(\mathcal{Q})} \left| \sum_{\mu \in \mathcal{Q}} \omega(\mu) \cdot (1 + \mathcal{O}(\epsilon)) \cdot W_z^z(\mu, \bar{\nu}) - \sum_{\mu \in \mathcal{S}} \tau(\mu) \cdot (1 - \mathcal{O}(\epsilon)) \cdot W_z^z(\mu, \bar{\nu}) \right| + \mathcal{O}(\frac{1}{\epsilon^{z-1}}) \cdot W_z^z(\nu, \bar{\nu}) \\ &= |(1 + \mathcal{O}(\epsilon))\mathcal{WB}(\mathcal{Q}, \bar{\nu}) - (1 - \mathcal{O}(\epsilon))\mathcal{WB}(\mathcal{S}, \bar{\nu})| + \mathcal{O}(\epsilon H^z) \\ &\leq \mathcal{O}(\epsilon) \cdot \mathcal{WB}(\mathcal{Q}, \bar{\nu}) + \mathcal{O}(\epsilon H^z) = \mathcal{O}(\epsilon) \cdot \mathcal{WB}(\mathcal{Q}, \bar{\nu}), \end{aligned}$$

where the first equality and the second equality come from the definition of $\mathcal{WB}(\cdot, \cdot)$, the first inequality follows from generalized triangle inequality, and the last equality is due to the fact that $H^z = \mathcal{O}(1) \cdot \text{OPT} \leq \mathcal{O}(1) \cdot \mathcal{WB}(\mathcal{Q}, \bar{\nu})$. By using Lemma 4.2 again, we have $\mathcal{WB}(\mathcal{Q}, \bar{\nu}) \leq (1 + \mathcal{O}(\epsilon)) \cdot \mathcal{WB}(\mathcal{Q}, \nu) + \mathcal{O}(\epsilon H^z)$; then, we obtain $|\mathcal{WB}(\mathcal{Q}, \nu) - \mathcal{WB}(\mathcal{S}, \nu)| \leq \mathcal{O}(\epsilon) \cdot \mathcal{WB}(\mathcal{Q}, \nu)$. \square

4.3 Algorithm Algorithm 2 aims to compute a solution for free-RWB on the input probability measure set \mathcal{Q} (as in (2.2)), and it leverages model reduction and coreset technique to accelerate the computation.

By model reduction, to solve free-RWB, we can compute free-AWB by updating the weights and locations alternatively. We pre-specify the number of iterations as `lter`. At each iteration, updating weights is finished by invoking fixed-AWB. Updating locations is a power mean problem; for a special case $z = 2$, it is a geometric mean problem [9].

By coreset technique, we can construct a small proxy \mathcal{S} (returned by Algorithm 1) anchored at a $\mathcal{O}(1)$ -approximate solution. For the q -th iteration, we assume $\mathcal{S} = \{\mu^{q^l}\}_{l \in [|\mathcal{S}|]}$, where $X^{q^l} := \{x_i^{q^l}\}_{i \in [n]}$ is the locations of μ^{q^l} . We can run algorithms on \mathcal{S} instead of on the original data set \mathcal{Q} , which can be very large. Thus, it can improve efficiency by reducing the data set size m . Besides, since coreset \mathcal{S} only works for local area $\mathcal{D}_{\tilde{\nu}}$, we reconstruct it if ν' is out of $\mathcal{D}_{\tilde{\nu}}$.

Algorithm 2 Algorithm for free-RWB

Input: Probability measure set \mathcal{Q} ,

$\mathcal{O}(1)$ -approximate solution $\tilde{\nu}$.

- 1: $\nu = \tilde{\nu}$, $q = 0$;
- 2: Construct a local coreset \mathcal{S} anchored at ν for free-RWB on \mathcal{Q} by Algorithm 1;
- 3: **for** $q < \text{lter}$ **do**
- 4: $q = q + 1$;
- 5: Compute the coupling set $\{\mathbf{P}_{\text{aug}}^l\}_{l \in [m]}$ of the fixed-AWB on \mathcal{Q} by invoking (3.12);
- 6: $\mathbf{b}' = (\mathbf{P}_{\text{aug}}^1)^T \mathbf{1} \in \mathbb{R}_+^{n+1}$;
- 7: $\nu' = \sum_{j=1}^n b'_j \delta_{y_j}$;
- 8: **if** $\nu' \in \mathcal{D}_{\tilde{\nu}}$ **then**
- 9: $b_j = b'_j$ for $j \in [n]$; ▷ update the weights of ν ;
- 10: **else**
- 11: $\nu = \sum_{j=1}^n b_j \delta_{y_j}$ and turn to Line 2;
- 12: **end if**
- 13: Compute $y'_j = \arg \min_y \sum_{l=1}^{|\mathcal{S}|} \tau(\mu^{q^l}) \sum_{i=1}^n P_{ij}^{q^l} \cdot \text{dist}^z(x_i^{q^l}, y)$ for all $j \in [n]$;
- 14: $\nu' = \sum_{j=1}^n b_j \delta_{y'_j}$;
- 15: **if** $\nu' \in \mathcal{D}_{\tilde{\nu}}$ **then**
- 16: $y_j = y'_j$ for $j \in [n]$; ▷ update the locations of ν ;
- 17: **else**
- 18: $\nu = \sum_{j=1}^n b_j \delta_{y_j}$ and turn to Line 2;
- 19: **end if**
- 20: **end for**

Output: $\nu = \sum_{j=1}^n b_j \delta_{y_j}$.

REMARK 4.3. *Actually, Algorithm 2 offers a framework for solving free-RWB. We can use the techniques in Frank-Wolfe algorithm [21, 23] to improve it in the future.*

5 Experiments

This section demonstrates the effectiveness of the free-RWB and the efficiency of the coreset technique. All the experiments were conducted on a server equipped with 2.40GHz Intel CPU, 128GB main memory, and Python 3.8. Due to space limitations, we only show part of the experimental results here. (More experiments can be found in Appendix.)

We evaluate our method on the MNIST [1] dataset, which is a popular handwritten benchmark with digits from 0 to 9. We select 3000 images. For the l -th image, we represent it by a measure $\mu^l = \sum_{i=1}^{60} a_i^l \delta_{x_i^l} \in \mathcal{P}(\mathcal{X})$ via k -means clustering. More specifically, we take 28×28 pixels as the input of clustering, and obtain 60 cluster centers $X^l = \{x_i^l\}_{i \in [60]}$ as the locations of μ^l ; the weight a_i^l is proportional to the total pixel number of this

Table 1: Comparisons of our free-RWB and the original WB algorithm under different noise intensity. We use ζ to denote the total mass of outliers, and the noise distribution (N.D.) is Gaussian distribution $\mathcal{N}(\cdot, \cdot)$.

ζ	N.D.	Our free-RWB			WB		
		runtime (\downarrow)	WD (\downarrow)	cost (\downarrow)	runtime (\downarrow)	WD (\downarrow)	cost (\downarrow)
0.1	$\mathcal{N}(20, 20^2)$	406.26 \pm 101.29	0.56 \pm 0.02	57.98 \pm 0.02	429.72 \pm 125.86	0.57 \pm 0.02	57.99 \pm 0.02
	$\mathcal{N}(40, 40^2)$	374.55 \pm 111.53	2.86 \pm 0.11	59.46 \pm 0.11	371.07 \pm 109.45	91.27 \pm 31.51	114.97 \pm 27.88
	$\mathcal{N}(60, 60^2)$	299.06 \pm 29.56	0.85 \pm 0.04	58.27 \pm 0.04	313.12 \pm 42.11	473.66 \pm 7.86	444.91 \pm 6.86
0.2	$\mathcal{N}(20, 20^2)$	434.46 \pm 71.85	2.50 \pm 0.09	59.47 \pm 0.09	465.89 \pm 105.96	2.56 \pm 0.09	59.52 \pm 0.09
	$\mathcal{N}(40, 40^2)$	462.63 \pm 109.26	15.78 \pm 3.13	59.81 \pm 1.01	448.58 \pm 67.21	382.56 \pm 6.81	335.22 \pm 6.47
	$\mathcal{N}(60, 60^2)$	460.43 \pm 66.94	3.71 \pm 0.12	59.22 \pm 0.26	481.08 \pm 56.36	1201.98 \pm 8.23	1054.11 \pm 7.66
0.3	$\mathcal{N}(20, 20^2)$	477.99 \pm 74.03	5.84 \pm 0.11	61.41 \pm 0.20	509.11 \pm 48.46	5.99 \pm 0.11	61.51 \pm 0.21
	$\mathcal{N}(40, 40^2)$	306.84 \pm 39.58	198.63 \pm 74.20	174.58 \pm 62.32	312.85 \pm 35.12	661.14 \pm 7.50	540.72 \pm 7.90
	$\mathcal{N}(60, 60^2)$	444.65 \pm 110.59	10.86 \pm 1.14	56.03 \pm 0.76	519.71 \pm 76.13	2093.29 \pm 10.88	1811.10 \pm 9.60

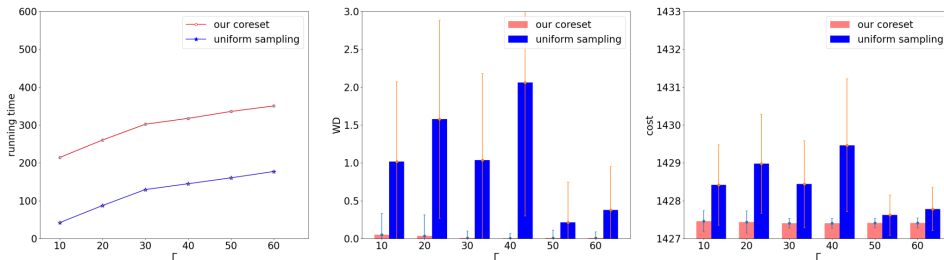


Figure 1: Comparisons of our coreset and uniform sampling. Γ is the sample size for each layer in our method.

cluster. Till now, we obtain a clean data set $\mathcal{Q} = \{\mu^l\}_{l \in [3000]}$. We assume \mathcal{Q}' is its corresponding noisy data set, which will be constructed later.

The method proposed by Le et al. [26] suffers from numerical instability caused by the KL-divergence regularization term. In almost all the instances here, it failed to produce results. Thus, we only compare our method with the original Wasserstein barycenter (WB) algorithm here.⁵

To measure the performance of our methods, we consider three criteria: (i) running time: the CPU time consumed by algorithms; (ii) WD: the Wasserstein distance between the barycenter computed on the noisy data set \mathcal{Q}' and the WB on the clean data set \mathcal{Q} ; (iii) cost: Let ν be the barycenter computed by some algorithm on the noisy data set \mathcal{Q}' . We define its cost as $WB(\mathcal{Q}, \nu)$. (Note that its cost is evaluated on the clean data set \mathcal{Q} .) We run 10 trials and record the average results.

First, to show the efficiency of our free-RWB, we add ζ mass of Gaussian noise to each measure $\mu^l \in \mathcal{Q}$ to obtain a noisy data set \mathcal{Q}' . Then, we compute barycenter by the original WB algorithm and our free-RWB on the noisy dataset respectively. The results in Table 3 show that our free-RWB can tackle outliers effectively under different noise intensity.

Then, we show the efficiency of our coreset technique in Figure 1. In this scenario, to obtain a noisy data set \mathcal{Q}' , we first add 0.1 mass of Gaussian noise from $\mathcal{N}(40, 40)$ to each measure $\mu^l \in \mathcal{Q}$, and then shift the locations of 300 images randomly according to the distribution $\mathcal{N}(0, 80)$. Throughout our experiments, we ensure that the total sample size of the uniform sampling method equals to the coreset size of our method. Our coreset method is much more time consuming. However, it performs well on the criteria WD and cost. Moreover, our method is more stable.

⁵The codes and full experiments (including the results on the other data sets and contrast experiments on the numerical instability issues [26]) are available at https://github.com/little-worm/iicllrr2023/blob/main/Full_experiments.pdf.

6 Conclusion and future work

In this paper, we study two types of RWB: fixed-RWB and free-RWB. Our fixed-RWB can be solved within $\mathcal{O}(\frac{mn^2}{\epsilon_+})$ time efficiently by reducing it as an LP; for free-RWB, we use model reduction and coresets technique to accelerate it. Obviously, our Algorithm 2 performs well in practice. In theory, we can guarantee that the output is a constant approximate solution. In the future, how to compute a $(1 + \epsilon)$ -approximate solution for $0 < \epsilon < 1$ is worth studying.

Acknowledgment

Thanks to Professor Ding for his help and instruction on this paper. “Data were provided (in part) by the Human Connectome Project, WU-Minn Consortium (Principal Investigators: David Van Essen and Kamil Ugurbil; 1U54MH091657) funded by the 16 NIH Institutes and Centers that support the NIH Blueprint for Neuroscience Research; and by the McDonnell Center for Systems Neuroscience at Washington University.”

Appendix

A Full Experiments

Here, we demonstrate the effectiveness of the fixed-RWB/free-RWB and the efficiency of the coresets technique. All the experiments were conducted on a server equipped with 2.40GHz Intel CPU, 128GB main memory, and Python 3.8.

We evaluate our method on three datasets: MNIST [1], ModelNet40 [40] and Human Connectome Project (HCP) [37].

MNIST: MNIST dataset [1] is a popular handwritten benchmark with digits from 0 to 9. We select 3000 images. For the l -th image, we represent it by a measure $\mu^l = \sum_{i=1}^{60} a_i^l \delta_{x_i^l} \in \mathcal{P}(\mathcal{X})$ via k -means clustering. More specifically, we take 28×28 pixels as the input of clustering, and obtain 60 cluster centers $X^l = \{x_i^l\}_{i \in [60]}$ as the locations of μ^l ; the weight a_i^l is proportional to the total pixel number of this cluster. Till now, we obtain a clean dataset $\mathcal{Q} = \{\mu^l\}_{l \in [3000]}$. We assume \mathcal{Q}' is its corresponding noisy dataset, which will be constructed for each dataset later.

ModelNet40: ModelNet40 [40] is a comprehensive clean collection of 3D CAD models. We choose 989 CAD models of chair. First, we convert these CAD models into point clouds. Then, each point cloud was grouped into $k = 60$ clusters; each cluster was represented by its cluster center; the weight of each center is proportional to the total number of points of the cluster. Then, we can obtain \mathcal{Q} and \mathcal{Q}' (as described in MNIST dataset).

Human Connectome Project (HCP): Human Connectome Project (HCP) [37] is a dataset of high-quality neuroimaging data in over 1100 healthy young adults, aged 22–35. We took 3000 3D brain images. For each image, its voxels were grouped into $k = 60$ clusters; each cluster was represented by its cluster center; the weight of each center is proportional to the total number of points of the cluster. Then, we can obtain \mathcal{Q} and \mathcal{Q}' (as described in MNIST dataset).

The method proposed by Le et al. [26] suffers from numerical instability caused by the KL-divergence regularization term. (This is illustrated in Appendix A.4.) In almost all the instances here, it failed to produce results. Thus, we only compare our method with the original Wasserstein barycenter (WB) algorithm here.⁶

To measure the performance of our methods, we consider three criteria: (i) running time: the CPU time consumed by algorithms; (ii) WD: the Wasserstein distance between the barycenter computed on the noisy dataset \mathcal{Q}' and the WB on the clean dataset \mathcal{Q} ; (iii) cost: Let ν be the barycenter computed by some algorithm on the noisy dataset \mathcal{Q}' . We define its cost as $WB(\mathcal{Q}, \nu)$. (Note that its cost is evaluated on the clean dataset \mathcal{Q} .) We run 10 trials and record the average results.

A.1 Experiments on MNIST Dataset This section shows the experimental result on MNIST dataset. First, to show the efficiency of our fixed-RWB/free-RWB, we add ζ mass of Gaussian noise to each measure $\mu^l \in \mathcal{Q}$ to

⁶The codes and full experiments (including the results on the other datasets and contrast experiments on the numerical instability issues [26]) are available at https://github.com/little-worm/iicllrr2023/blob/main/Full_experiments.pdf.

obtain a noisy dataset \mathcal{Q}' . Then, we compute barycenter by the original fixed-support/free-support WB algorithm and our fixed-RWB/free-RWB on the noisy dataset respectively. The results in Table 2/Table 3 show that our fixed-RWB/free-RWB can tackle outliers effectively under different noise intensity.

Table 2: Comparisons of our fixed-RWB and the original fixed-support WB algorithm under different noise intensity on MNIST. We use ζ to denote the total mass of outliers, and the noise distribution (N.D.) is Gaussian distribution $\mathcal{N}(\cdot, \cdot)$.

ζ	N.D.	Our fixed-RWB			WB		
		runtime (\downarrow)	WD (\downarrow)	cost (\downarrow)	runtime (\downarrow)	WD (\downarrow)	cost (\downarrow)
0.1	$\mathcal{N}(20, 20^2)$	89.38 \pm 24.89	0.14 \pm 0.00	3.54 \pm 0.00	99.11 \pm 31.32	0.14 \pm 0.00	3.54 \pm 0.00
	$\mathcal{N}(40, 40^2)$	80.83 \pm 23.43	13.73 \pm 0.10	23.06 \pm 0.11	74.42 \pm 13.06	21.92 \pm 0.23	32.25 \pm 0.26
	$\mathcal{N}(60, 60^2)$	66.78 \pm 14.84	88.49 \pm 1.51	86.17 \pm 1.32	75.15 \pm 10.62	189.53 \pm 1.36	175.33 \pm 1.20
0.2	$\mathcal{N}(20, 20^2)$	67.96 \pm 24.50	0.29 \pm 0.01	4.52 \pm 0.00	96.60 \pm 24.53	0.30 \pm 0.01	4.53 \pm 0.00
	$\mathcal{N}(40, 40^2)$	100.53 \pm 25.94	25.42 \pm 0.19	38.18 \pm 0.22	119.50 \pm 30.14	44.04 \pm 0.24	60.19 \pm 0.29
	$\mathcal{N}(60, 60^2)$	77.53 \pm 17.41	171.08 \pm 1.65	165.06 \pm 1.53	90.63 \pm 19.26	386.12 \pm 2.05	365.86 \pm 1.92
0.3	$\mathcal{N}(20, 20^2)$	85.55 \pm 18.26	0.57 \pm 0.01	5.25 \pm 0.00	106.25 \pm 38.59	0.58 \pm 0.01	5.26 \pm 0.00
	$\mathcal{N}(40, 40^2)$	103.50 \pm 27.60	27.50 \pm 0.18	41.44 \pm 0.21	102.17 \pm 34.68	69.02 \pm 0.35	89.88 \pm 0.42
	$\mathcal{N}(60, 60^2)$	98.17 \pm 17.41	190.22 \pm 1.72	197.55 \pm 1.76	68.74 \pm 14.46	552.93 \pm 2.79	563.60 \pm 2.82

Table 3: Comparisons of our free-RWB and the original free-support WB algorithm under different noise intensity on MNIST. We use ζ to denote the total mass of outliers, and the noise distribution (N.D.) is Gaussian distribution $\mathcal{N}(\cdot, \cdot)$.

ζ	N.D.	Our free-RWB			WB		
		runtime (\downarrow)	WD (\downarrow)	cost (\downarrow)	runtime (\downarrow)	WD (\downarrow)	cost (\downarrow)
0.1	$\mathcal{N}(20, 20^2)$	406.26 \pm 101.29	0.56 \pm 0.02	57.98 \pm 0.02	429.72 \pm 125.86	0.57 \pm 0.02	57.99 \pm 0.02
	$\mathcal{N}(40, 40^2)$	374.55 \pm 111.53	2.86 \pm 0.11	59.46 \pm 0.11	371.07 \pm 109.45	91.27 \pm 31.51	114.97 \pm 27.88
	$\mathcal{N}(60, 60^2)$	299.06 \pm 29.56	0.85 \pm 0.04	58.27 \pm 0.04	313.12 \pm 42.11	473.66 \pm 7.86	444.91 \pm 6.86
0.2	$\mathcal{N}(20, 20^2)$	434.46 \pm 71.85	2.50 \pm 0.09	59.47 \pm 0.09	465.89 \pm 105.96	2.56 \pm 0.09	59.52 \pm 0.09
	$\mathcal{N}(40, 40^2)$	462.63 \pm 109.26	15.78 \pm 3.13	59.81 \pm 1.01	448.58 \pm 67.21	382.56 \pm 6.81	335.22 \pm 6.47
	$\mathcal{N}(60, 60^2)$	460.43 \pm 66.94	3.71 \pm 0.12	59.22 \pm 0.26	481.08 \pm 56.36	1201.98 \pm 8.23	1054.11 \pm 7.66
0.3	$\mathcal{N}(20, 20^2)$	477.99 \pm 74.03	5.84 \pm 0.11	61.41 \pm 0.20	509.11 \pm 48.46	5.99 \pm 0.11	61.51 \pm 0.21
	$\mathcal{N}(40, 40^2)$	306.84 \pm 39.58	198.63 \pm 74.20	174.58 \pm 62.32	312.85 \pm 35.12	661.14 \pm 7.50	540.72 \pm 7.90
	$\mathcal{N}(60, 60^2)$	444.65 \pm 110.59	10.86 \pm 1.14	56.03 \pm 0.76	519.71 \pm 76.13	2093.29 \pm 10.88	1811.10 \pm 9.60

Then, we show the efficiency of our coreset technique in Figures 2 to 10. In this scenario, to obtain a noisy dataset \mathcal{Q}' , we first add 0.1 mass of Gaussian noise from $\mathcal{N}(40, 40)$ to each measure $\mu^l \in \mathcal{Q}$, and then shift the locations of several images randomly according to a distribution $\mathcal{N}(0, \cdot)$. Throughout our experiments, we ensure that the total sample size of the uniform sampling method equals to the coreset size of our method. Γ is the sample size for each layer in our method. Our coreset method is much more time consuming. However, it performs well on the criteria WD and cost. Moreover, our method is more stable.

A.2 Experiments on HCP Dataset This section shows the experimental result on HCP dataset. First, to show the efficiency of our fixed-RWB/free-RWB, we add ζ mass of Gaussian noise to each measure $\mu^l \in \mathcal{Q}$ to obtain a noisy dataset \mathcal{Q}' . Then, we compute barycenter by the original fixed-support/free-support WB algorithm and our fixed-RWB/free-RWB on the noisy dataset respectively. The results in Table 4/Table 5 show that our fixed-RWB/free-RWB can tackle outliers effectively under different noise intensity.

Then, we show the efficiency of our coreset technique in Figures 11 to 19. In this scenario, to obtain a noisy dataset \mathcal{Q}' , we first add 0.1 mass of Gaussian noise from $\mathcal{N}(40, 40)$ to each measure $\mu^l \in \mathcal{Q}$, and then shift the

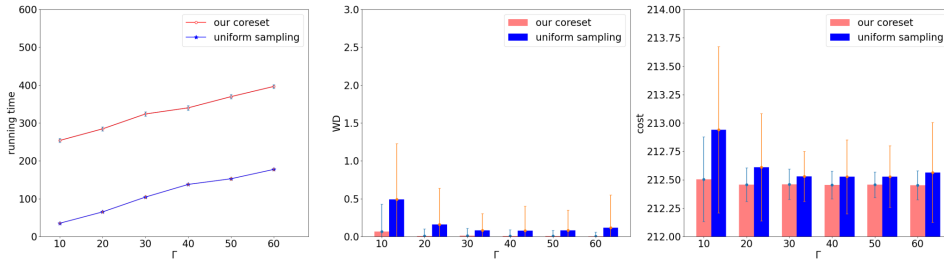


Figure 2: Comparisons of our coresets and uniform sampling on MNIST. Shift locations of 100 images according to distribution $\mathcal{N}(0, 40)$.

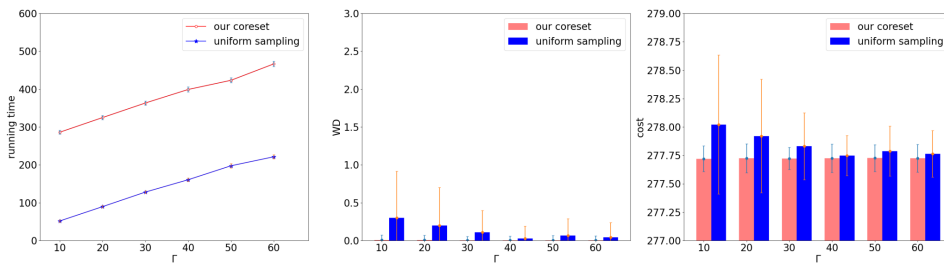


Figure 3: Comparisons of our coresets and uniform sampling on MNIST. Shift locations of 200 images according to distribution $\mathcal{N}(0, 40)$.

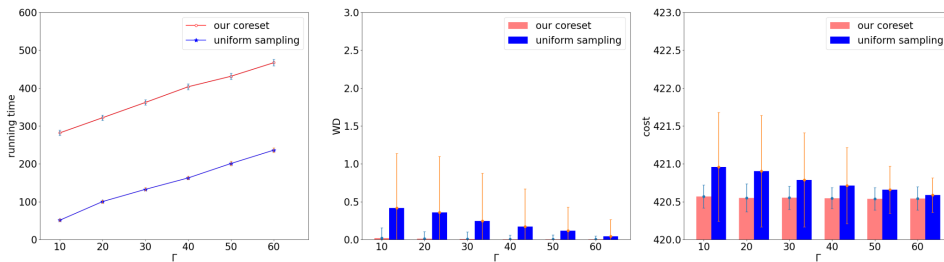


Figure 4: Comparisons of our coresets and uniform sampling on MNIST. Shift locations of 300 images according to distribution $\mathcal{N}(0, 40)$.

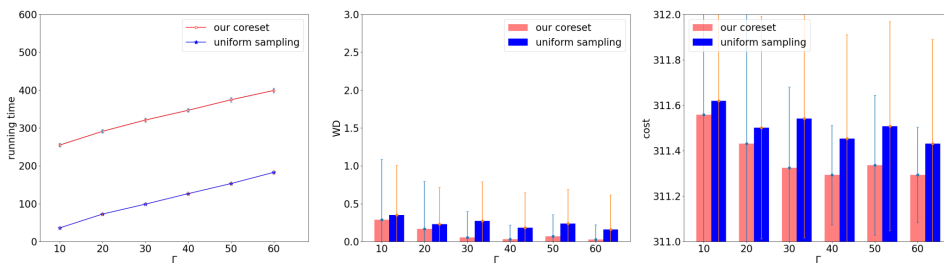


Figure 5: Comparisons of our coresets and uniform sampling on MNIST. Shift locations of 100 images according to distribution $\mathcal{N}(0, 60)$.

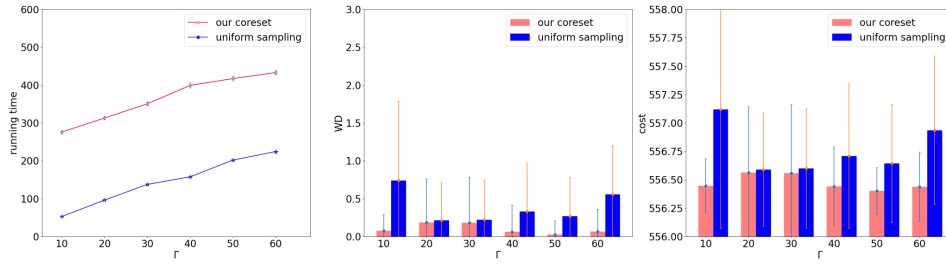


Figure 6: Comparisons of our coresets and uniform sampling on MNIST. Shift locations of 200 images according to distribution $\mathcal{N}(0, 60)$.

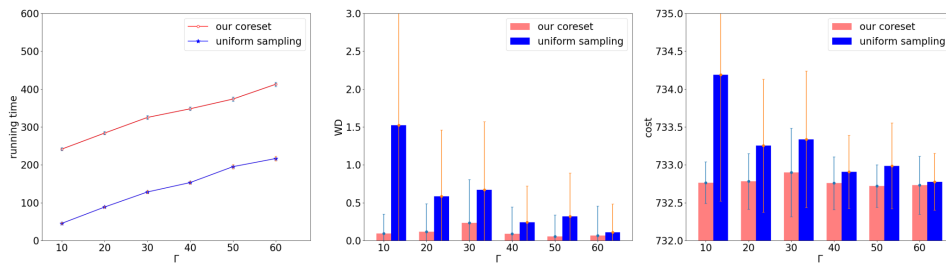


Figure 7: Comparisons of our coresets and uniform sampling on MNIST. Shift locations of 300 images according to distribution $\mathcal{N}(0, 60)$.

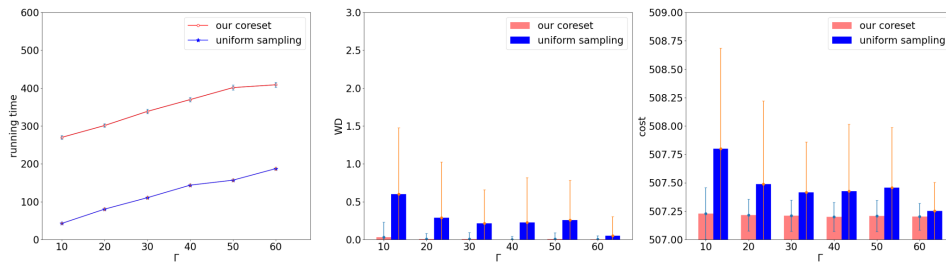


Figure 8: Comparisons of our coresets and uniform sampling on MNIST. Shift locations of 100 images according to distribution $\mathcal{N}(0, 80)$.

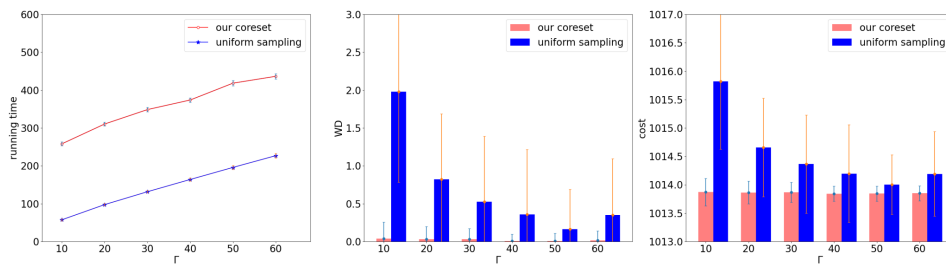


Figure 9: Comparisons of our coresets and uniform sampling on MNIST. Shift locations of 200 images according to distribution $\mathcal{N}(0, 80)$.

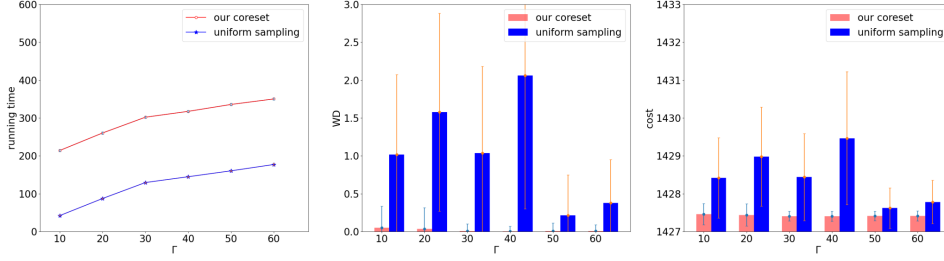


Figure 10: Comparisons of our coreset and uniform sampling on MNIST. Shift locations of 300 images according to distribution $\mathcal{N}(0, 80)$.

Table 4: Comparisons of our fixed-RWB and the original fixed-support WB algorithm under different noise intensity on HCP. We use ζ to denote the total mass of outliers, and the noise distribution (N.D.) is Gaussian distribution $\mathcal{N}(\cdot, \cdot)$.

ζ	N.D.	Our fixed-RWB			WB		
		runtime (\downarrow)	WD (\downarrow)	cost (\downarrow)	runtime (\downarrow)	WD (\downarrow)	cost (\downarrow)
0.1	$\mathcal{N}(50, 50^2)$	101.50 \pm 35.27	4.98 \pm 0.12	97.39 \pm 0.05	92.71 \pm 25.00	5.20 \pm 0.11	97.34 \pm 0.05
	$\mathcal{N}(100, 100^2)$	84.28 \pm 29.66	89.45 \pm 1.39	179.87 \pm 1.37	105.27 \pm 25.10	321.63 \pm 1.72	404.51 \pm 1.67
	$\mathcal{N}(150, 150^2)$	83.36 \pm 6.68	82.40 \pm 3.90	176.28 \pm 3.94	89.49 \pm 24.22	2039.19 \pm 7.51	2134.79 \pm 7.46
0.2	$\mathcal{N}(50, 50^2)$	61.77 \pm 16.90	10.15 \pm 0.23	96.36 \pm 0.05	65.90 \pm 16.08	10.78 \pm 0.24	96.24 \pm 0.05
	$\mathcal{N}(100, 100^2)$	77.48 \pm 17.16	169.68 \pm 1.28	256.04 \pm 1.29	72.97 \pm 18.30	718.88 \pm 3.54	788.35 \pm 3.40
	$\mathcal{N}(150, 150^2)$	52.19 \pm 3.50	231.62 \pm 5.89	327.27 \pm 6.05	49.86 \pm 1.99	4505.75 \pm 18.61	4584.84 \pm 18.32
0.3	$\mathcal{N}(50, 50^2)$	95.91 \pm 33.15	15.40 \pm 0.09	95.66 \pm 0.04	107.73 \pm 22.91	16.60 \pm 0.10	95.55 \pm 0.05
	$\mathcal{N}(100, 100^2)$	93.63 \pm 27.43	184.54 \pm 2.30	268.10 \pm 2.34	99.77 \pm 25.78	1180.03 \pm 6.22	1227.38 \pm 6.04
	$\mathcal{N}(150, 150^2)$	49.84 \pm 3.15	422.77 \pm 6.48	521.64 \pm 6.48	50.87 \pm 5.31	7182.62 \pm 16.07	7211.00 \pm 15.77

Table 5: Comparisons of our free-RWB and the original free-support WB algorithm under different noise intensity on HCP. We use ζ to denote the total mass of outliers, and the noise distribution (N.D.) is Gaussian distribution $\mathcal{N}(\cdot, \cdot)$.

ζ	N.D.	Our free-RWB			WB		
		runtime (\downarrow)	WD (\downarrow)	cost (\downarrow)	runtime (\downarrow)	WD (\downarrow)	cost (\downarrow)
0.1	$\mathcal{N}(50, 50^2)$	364.40 \pm 55.35	2.79 \pm 0.10	924.84 \pm 0.13	391.94 \pm 46.67	3.19 \pm 0.10	924.63 \pm 0.17
	$\mathcal{N}(100, 100^2)$	362.76 \pm 41.85	2.53 \pm 0.08	925.81 \pm 0.16	393.62 \pm 51.49	1428.06 \pm 53.70	1758.54 \pm 36.74
	$\mathcal{N}(150, 150^2)$	377.66 \pm 68.12	0.09 \pm 0.01	927.67 \pm 0.03	390.97 \pm 72.66	4912.27 \pm 52.62	4581.39 \pm 48.59
0.2	$\mathcal{N}(50, 50^2)$	385.24 \pm 74.60	11.78 \pm 0.56	910.16 \pm 0.74	402.37 \pm 74.39	14.10 \pm 0.62	906.11 \pm 0.72
	$\mathcal{N}(100, 100^2)$	392.26 \pm 73.57	9.96 \pm 0.32	918.17 \pm 1.02	385.29 \pm 50.78	3962.80 \pm 179.01	3409.19 \pm 147.24
	$\mathcal{N}(150, 150^2)$	347.45 \pm 27.78	0.30 \pm 0.02	927.10 \pm 0.06	400.30 \pm 25.87	12873.93 \pm 88.97	11040.97 \pm 78.38
0.3	$\mathcal{N}(50, 50^2)$	342.88 \pm 24.33	30.53 \pm 0.50	867.25 \pm 1.57	377.99 \pm 45.68	38.19 \pm 0.77	847.05 \pm 2.33
	$\mathcal{N}(100, 100^2)$	347.99 \pm 43.53	30.51 \pm 7.15	889.46 \pm 4.19	400.05 \pm 40.38	7414.53 \pm 51.70	5896.24 \pm 53.92
	$\mathcal{N}(150, 150^2)$	43.53 \pm 56.00	7.15 \pm 0.03	4.19 \pm 0.09	40.38 \pm 26.55	51.70 \pm 87.81	53.92 \pm 76.20

locations of several images randomly according to a distribution $\mathcal{N}(0, \cdot)$. Throughout our experiments, we ensure that the total sample size of the uniform sampling method equals to the coreset size of our method. Γ is the sample size for each layer in our method. Our coreset method is much more time consuming. However, it performs well on the criteria WD and cost. Moreover, our method is more stable. (The results of our coreset method perform well with high probability, so it is reasonable that our method performs worse than uniform sampling with small probability.)

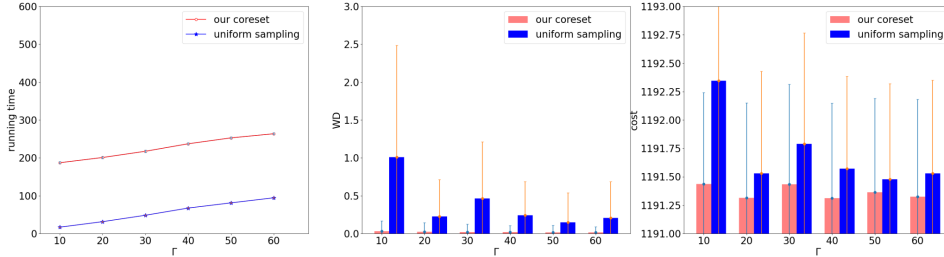


Figure 11: Comparisons of our coreset and uniform sampling on HCP. Shift locations of 100 brains according to distribution $\mathcal{N}(0, 50)$.

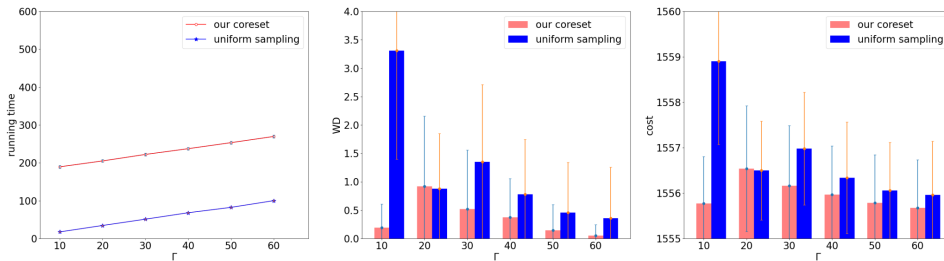


Figure 12: Comparisons of our coreset and uniform sampling on HCP. Shift locations of 200 brains according to distribution $\mathcal{N}(0, 50)$.

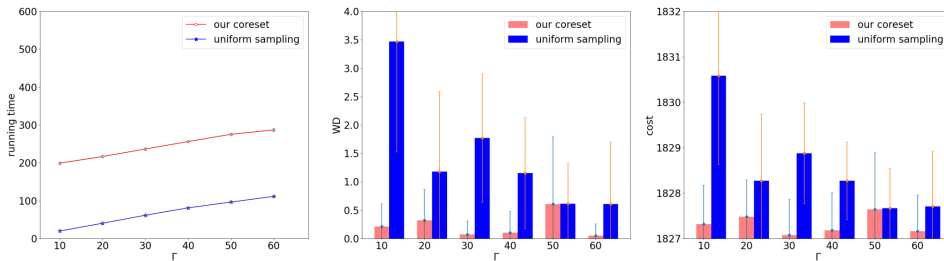


Figure 13: Comparisons of our coreset and uniform sampling on HCP. Shift locations of 300 brains according to distribution $\mathcal{N}(0, 50)$.

A.3 Experiments on ModelNet40 Dataset This section shows the experimental result on ModelNet40 dataset. First, to show the efficiency of our fixed-RWB/free-RWB, we add ζ mass of Gaussian noise to each measure $\mu^l \in \mathcal{Q}$ to obtain a noisy dataset \mathcal{Q}' . Then, we compute barycenter by the original fixed-support/free-support WB algorithm and our fixed-RWB/free-RWB on the noisy dataset respectively. The results in Table 6/Table 7 show

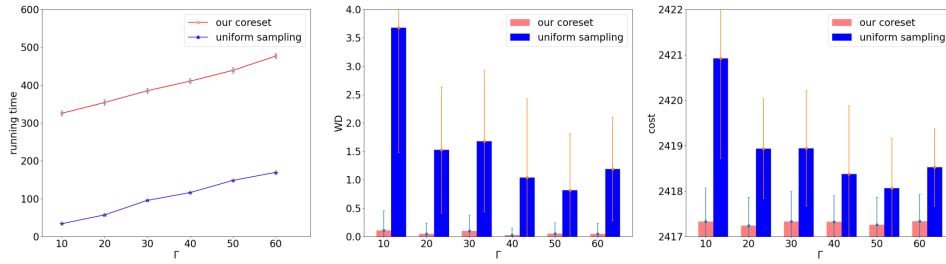


Figure 14: Comparisons of our coreset and uniform sampling on HCP. Shift locations of 100 brains according to distribution $\mathcal{N}(0, 100)$.

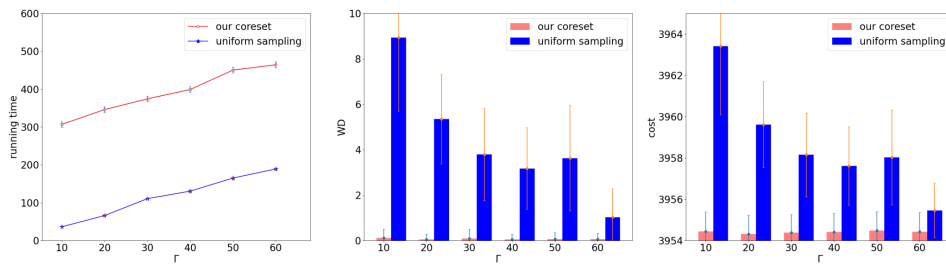


Figure 15: Comparisons of our coreset and uniform sampling on HCP. Shift locations of 200 brains according to distribution $\mathcal{N}(0, 100)$.

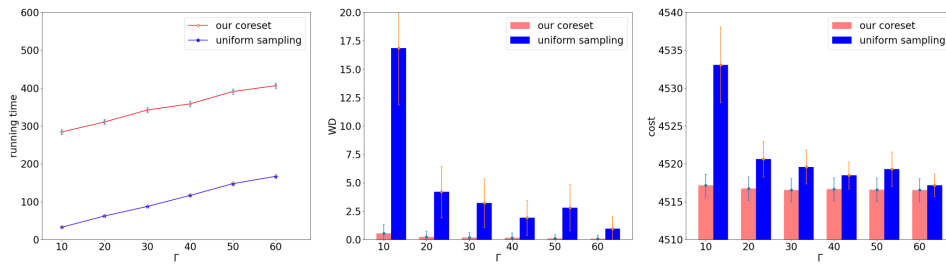


Figure 16: Comparisons of our coreset and uniform sampling on HCP. Shift locations of 300 brains according to distribution $\mathcal{N}(0, 100)$.

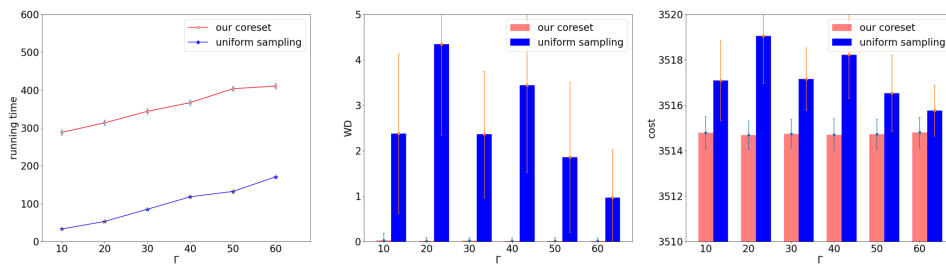


Figure 17: Comparisons of our coreset and uniform sampling on HCP. Shift locations of 100 brains according to distribution $\mathcal{N}(0, 150)$.

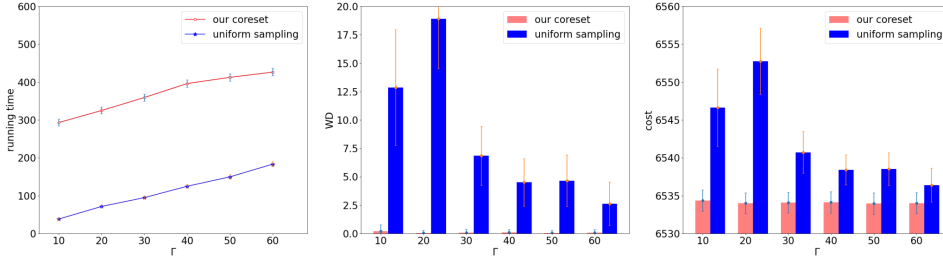


Figure 18: Comparisons of our coresets and uniform sampling on HCP. Shift locations of 200 brains according to distribution $\mathcal{N}(0, 150)$.

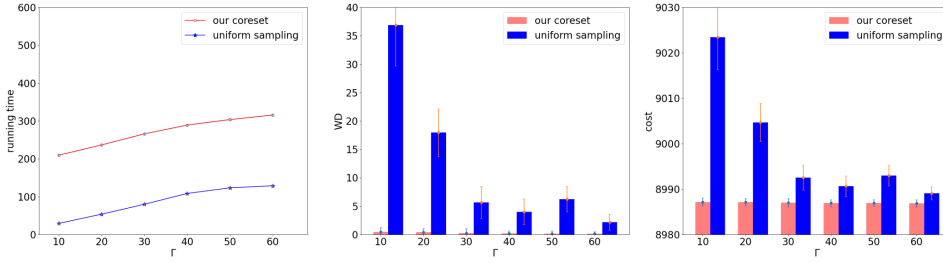


Figure 19: Comparisons of our coresets and uniform sampling on HCP. Shift locations of 300 brains according to distribution $\mathcal{N}(0, 150)$.

that our fixed-RWB/free-RWB can tackle outliers effectively under different noise intensity. In our experiments, we can only obtain a local approximate solution, the solution is somewhat random. Thus, it is reasonable that our method obtain worse result when the noise intensity is small.

Then, we show the efficiency of our coresets technique in Figures 20 to 28. In this scenario, to obtain a noisy dataset \mathcal{Q}' , we first add 0.1 mass of Gaussian noise from $\mathcal{N}(40, 40)$ to each measure $\mu^l \in \mathcal{Q}$, and then shift the locations of several images randomly according to a distribution $\mathcal{N}(0, \cdot)$. Throughout our experiments, we ensure that the total sample size of the uniform sampling method equals to the coresets size of our method. Γ is the sample size for each layer in our method. Our coresets method is much more time consuming. However, it performs well on the criteria WD and cost. Moreover, our method is more stable. (The results of our coresets method perform well with high probability, so it is reasonable that our method performs worse than uniform sampling with small probability.)

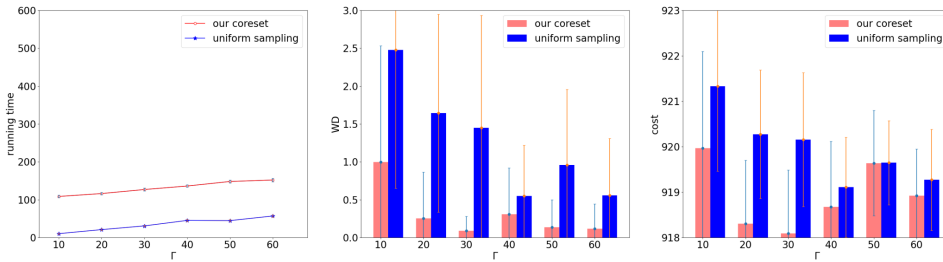


Figure 20: Comparisons of our coresets and uniform sampling on ModelNet40. Shift locations of 30 CAD models according to distribution $\mathcal{N}(0, 50)$.

Table 6: Comparisons of our fixed-RWB and the original fixed-support WB algorithm under different noise intensity on ModelNet40. We use ζ to denote the total mass of outliers, and the noise distribution (N.D.) is Gaussian distribution $\mathcal{N}(\cdot, \cdot)$.

ζ	N.D.	Our fixed-RWB			WB		
		runtime (\downarrow)	WD (\downarrow)	cost (\downarrow)	runtime (\downarrow)	WD (\downarrow)	cost (\downarrow)
0.1	$\mathcal{N}(50, 50^2)$	32.63 \pm 11.52	73.57 \pm 0.58	187.15 \pm 0.48	34.98 \pm 9.08	79.87 \pm 0.73	192.85 \pm 0.56
	$\mathcal{N}(100, 100^2)$	10.72 \pm 43.08	7.87 \pm 572.59	8.08 \pm 697.28	36.17 \pm 37.89	1172.51 \pm 3438.73	1278.68 \pm 3560.87
	$\mathcal{N}(150, 150^2)$	31.16 \pm 5.56	172.03 \pm 1.14	259.79 \pm 1.09	32.70 \pm 7.09	194.93 \pm 1.53	280.03 \pm 1.46
0.2	$\mathcal{N}(50, 50^2)$	32.37 \pm 6.97	1141.13 \pm 11.48	1242.84 \pm 11.41	33.31 \pm 6.10	2677.97 \pm 9.06	2760.90 \pm 8.88
	$\mathcal{N}(100, 100^2)$	38.34 \pm 9.18	1456.09 \pm 24.07	1583.98 \pm 24.01	37.31 \pm 11.37	7526.14 \pm 50.15	7638.26 \pm 50.09
	$\mathcal{N}(150, 150^2)$	32.30 \pm 8.32	276.55 \pm 3.00	344.85 \pm 2.82	32.48 \pm 8.99	324.69 \pm 3.40	388.14 \pm 3.08
0.3	$\mathcal{N}(50, 50^2)$	40.42 \pm 8.82	1368.73 \pm 16.04	1465.01 \pm 16.19	43.17 \pm 10.26	4314.01 \pm 25.69	4335.73 \pm 24.59
	$\mathcal{N}(100, 100^2)$	23.20 \pm 1.56	2283.81 \pm 41.22	2402.69 \pm 41.07	21.27 \pm 1.38	12023.66 \pm 31.14	12025.97 \pm 30.12
	$\mathcal{N}(150, 150^2)$	38.18 \pm 11.32	2279.04 \pm 27.75	2398.06 \pm 27.65	35.47 \pm 6.61	12032.18 \pm 40.15	12034.24 \pm 38.74

Table 7: Comparisons of our free-RWB and the original free-support WB algorithm under different noise intensity on ModelNet40. We use ζ to denote the total mass of outliers, and the noise distribution (N.D.) is Gaussian distribution $\mathcal{N}(\cdot, \cdot)$.

ζ	N.D.	Our free-RWB			WB		
		runtime (\downarrow)	WD (\downarrow)	cost (\downarrow)	runtime (\downarrow)	WD (\downarrow)	cost (\downarrow)
0.1	$\mathcal{N}(50, 50^2)$	165.92 \pm 25.89	161.05 \pm 85.74	700.58 \pm 37.09	160.59 \pm 14.37	305.74 \pm 28.49	759.37 \pm 22.66
	$\mathcal{N}(100, 100^2)$	147.06 \pm 18.13	5.17 \pm 0.31	694.28 \pm 1.88	154.87 \pm 14.97	2727.47 \pm 63.60	2524.60 \pm 54.60
	$\mathcal{N}(150, 150^2)$	162.39 \pm 12.54	0.34 \pm 0.05	697.43 \pm 0.13	159.90 \pm 14.85	6485.18 \pm 98.90	5754.88 \pm 81.64
0.2	$\mathcal{N}(50, 50^2)$	147.41 \pm 25.81	1047.55 \pm 42.76	1143.70 \pm 32.79	148.08 \pm 23.28	1036.94 \pm 27.18	1132.61 \pm 22.44
	$\mathcal{N}(100, 100^2)$	133.21 \pm 10.56	472.29 \pm 507.73	918.99 \pm 306.73	147.36 \pm 10.85	6725.00 \pm 75.05	5554.06 \pm 60.25
	$\mathcal{N}(150, 150^2)$	156.13 \pm 21.13	2.06 \pm 0.18	697.74 \pm 0.34	178.76 \pm 27.98	16143.00 \pm 226.85	13870.42 \pm 199.02
0.3	$\mathcal{N}(50, 50^2)$	162.40 \pm 13.90	1899.46 \pm 46.76	1651.95 \pm 35.70	161.80 \pm 21.29	1836.57 \pm 35.69	1604.22 \pm 28.64
	$\mathcal{N}(100, 100^2)$	160.68 \pm 13.73	2498.13 \pm 751.33	2245.65 \pm 543.33	203.94 \pm 20.47	11554.34 \pm 149.35	9428.57 \pm 131.31
	$\mathcal{N}(150, 150^2)$	157.10 \pm 24.86	5.05 \pm 0.30	698.02 \pm 0.61	211.04 \pm 30.49	26774.86 \pm 243.22	23069.52 \pm 222.73

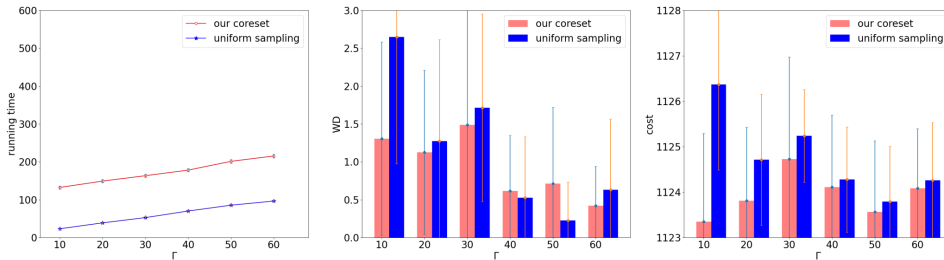


Figure 21: Comparisons of our coreset and uniform sampling on ModelNet40. Shift locations of 60 CAD models according to distribution $\mathcal{N}(0, 50)$.

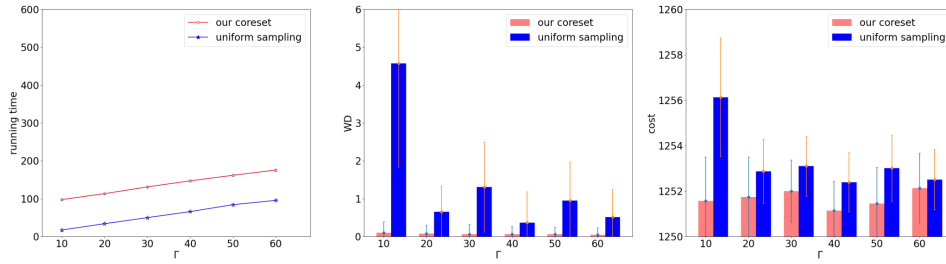


Figure 22: Comparisons of our coreset and uniform sampling on ModelNet40. Shift locations of 90 CAD models according to distribution $\mathcal{N}(0, 50)$.

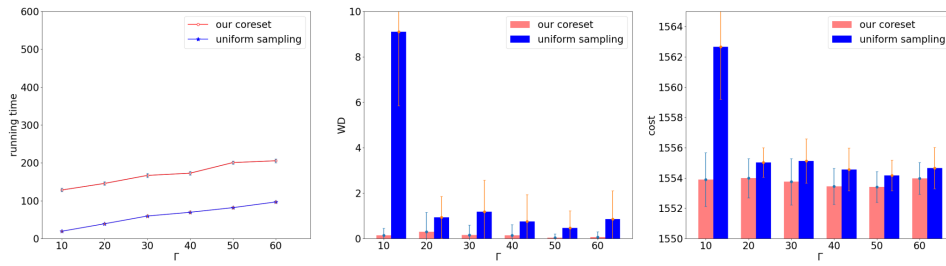


Figure 23: Comparisons of our coreset and uniform sampling on ModelNet40. Shift locations of 30 CAD models according to distribution $\mathcal{N}(0, 100)$.

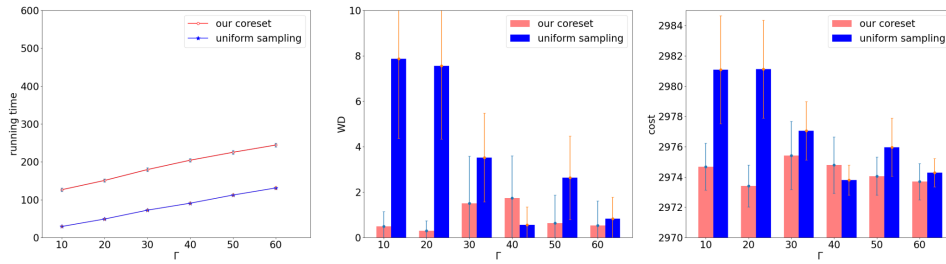


Figure 24: Comparisons of our coreset and uniform sampling on ModelNet40. Shift locations of 60 CAD models according to distribution $\mathcal{N}(0, 100)$.

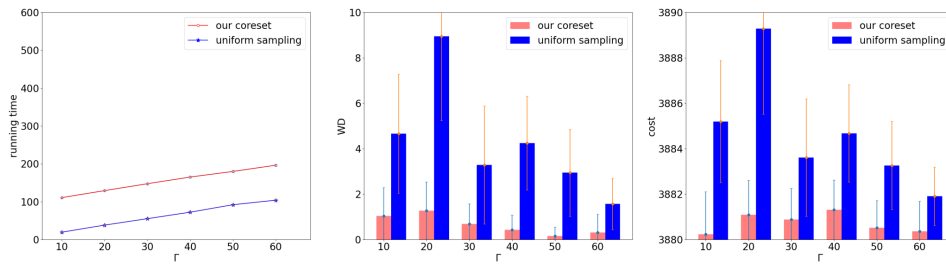


Figure 25: Comparisons of our coreset and uniform sampling on ModelNet40. Shift locations of 90 CAD models according to distribution $\mathcal{N}(0, 100)$.

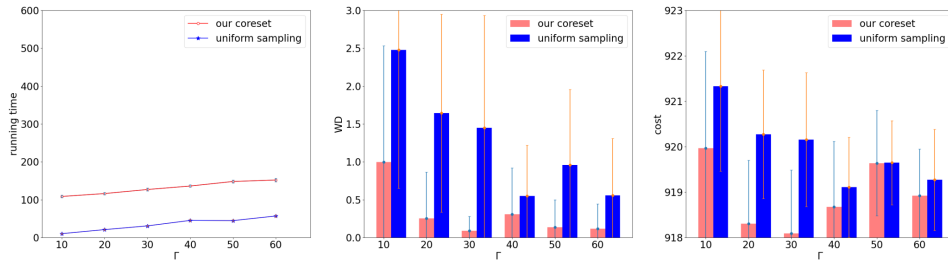


Figure 26: Comparisons of our coreset and uniform sampling on ModelNet40. Shift locations of 30 CAD models according to distribution $\mathcal{N}(0, 150)$.

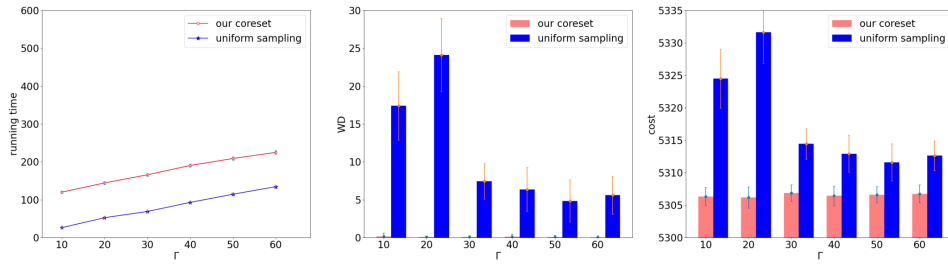


Figure 27: Comparisons of our coreset and uniform sampling on ModelNet40. Shift locations of 60 CAD models according to distribution $\mathcal{N}(0, 150)$.

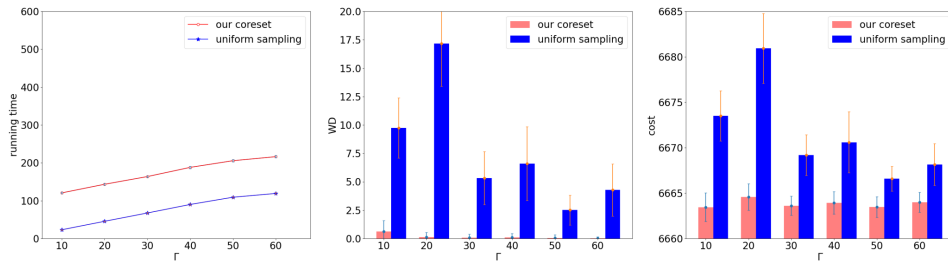


Figure 28: Comparisons of our coreset and uniform sampling on ModelNet40. Shift locations of 90 CAD models according to distribution $\mathcal{N}(0, 150)$.

A.4 Numerical Instability of Le et al. [26] In this section, we perform experiments on MNIST dataset to illustrate the numerical instability of Le et al. [26]. We select 300 images and obtain a clean dataset \mathcal{Q} . We add $\zeta = 0.2$ mass of Gaussian noise from $\mathcal{N}(40, \cdot)$ to each measure $\mu^l \in \mathcal{Q}$ to obtain a noisy dataset \mathcal{Q}' . Then, we compute barycenter by the original fixed-support WB algorithm and our fixed-RWB on the noisy dataset respectively. The results in the following table show that the method in [26] suffers from numerical instability. The symbol # denotes that we cannot compute the result due to numerical instability problem.

N.D.	method	runtime (\downarrow)	WD (\downarrow)	cost (\downarrow)
$\mathcal{N}(40, 0^2)$	our fixed-RWB	5.06	178.99	181.66
	fixed-support WB	5.23	179.62	182.29
	UOT ($\gamma = 1$)	2.34	332.58	331.17
	UOT ($\gamma = 4$)	2.34	246.93	248.12
	UOT ($\gamma = 16$)	2.34	198.82	199.93
	UOT ($\gamma = 64$)	2.33	181.89	182.59
	UOT ($\gamma = 256$)	2.33	177.15	177.75
	UOT ($\gamma = 1024$)	2.51	175.93	176.50
$\mathcal{N}(40, 5^2)$	our fixed-RWB	4.61	170.53	181.79
	fixed-support WB	4.24	172.74	184.04
	UOT ($\gamma = 1$)	2.29	6.55	9.49
	UOT ($\gamma = 4$)	2.17	32.63	37.17
	UOT ($\gamma = 16$)	2.18	201.32	212.21
	UOT ($\gamma = 64$)	2.25	379.00	390.25
	UOT ($\gamma = 256$)	2.23	452.12	463.62
	UOT ($\gamma = 1024$)	2.22	474.26	485.96
$\mathcal{N}(40, 10^2)$	our fixed-RWB	5.19	132.14	136.37
	fixed-support WB	3.42	157.34	161.61
	UOT ($\gamma = 1$)	#	#	#
	UOT ($\gamma = 4$)	#	#	#
	UOT ($\gamma = 16$)	#	#	#
	UOT ($\gamma = 64$)	#	#	#
	UOT ($\gamma = 256$)	#	#	#
	UOT ($\gamma = 1024$)	#	#	#
$\mathcal{N}(40, 15^2)$	our fixed-RWB	6.81	60.66	72.76
	fixed-support WB	3.51	124.52	139.82
	UOT ($\gamma = 1$)	#	#	#
	UOT ($\gamma = 4$)	#	#	#
	UOT ($\gamma = 16$)	#	#	#
	UOT ($\gamma = 64$)	#	#	#
	UOT ($\gamma = 256$)	#	#	#
	UOT ($\gamma = 1024$)	#	#	#
$\mathcal{N}(40, 20^2)$	our fixed-RWB	7.57	48.39	50.94
	fixed-support WB	3.66	130.31	129.04
	UOT ($\gamma = 1$)	#	#	#
	UOT ($\gamma = 4$)	#	#	#
	UOT ($\gamma = 16$)	#	#	#
	UOT ($\gamma = 256$)	#	#	#

Continued on next page

– continued from previous page

N.D.	method	runtime (\downarrow)	WD (\downarrow)	cost (\downarrow)
	UOT ($\gamma = 1024$)	#	#	#
	our fixed-RWB	4.18	39.79	42.23
	fixed-support WB	4.37	114.63	116.23
$\mathcal{N}(40, 25^2)$	UOT ($\gamma = 1$)	#	#	#
	UOT ($\gamma = 4$)	#	#	#
	UOT ($\gamma = 16$)	#	#	#
	UOT ($\gamma = 64$)	#	#	#
	UOT ($\gamma = 256$)	#	#	#
	UOT ($\gamma = 1024$)	#	#	#
		our fixed-RWB	7.59	35.06
	fixed-support WB	8.75	127.58	112.89
$\mathcal{N}(40, 30^2)$	UOT ($\gamma = 1$)	#	#	#
	UOT ($\gamma = 4$)	#	#	#
	UOT ($\gamma = 16$)	#	#	#
	UOT ($\gamma = 64$)	#	#	#
	UOT ($\gamma = 256$)	#	#	#
	UOT ($\gamma = 1024$)	#	#	#
		our fixed-RWB	8.83	20.71
	fixed-support WB	6.61	100.41	103.10
$\mathcal{N}(40, 35^2)$	UOT ($\gamma = 1$)	#	#	#
	UOT ($\gamma = 4$)	#	#	#
	UOT ($\gamma = 16$)	#	#	#
	UOT ($\gamma = 64$)	#	#	#
	UOT ($\gamma = 256$)	#	#	#
	UOT ($\gamma = 1024$)	#	#	#
		our fixed-RWB	5.13	12.55
	fixed-support WB	6.22	108.43	104.04
$\mathcal{N}(40, 40^2)$	UOT ($\gamma = 1$)	#	#	#
	UOT ($\gamma = 4$)	#	#	#
	UOT ($\gamma = 16$)	#	#	#
	UOT ($\gamma = 64$)	#	#	#
	UOT ($\gamma = 256$)	#	#	#
	UOT ($\gamma = 1024$)	#	#	#

B Other preliminaries

DEFINITION B.1. (DOUBLING DIMENSION [17]) *The doubling dimension of metric space $(\mathcal{X}, \text{dist})$ is the least d_{dim} such that every ball with radius $2r$ can be covered by at most $2^{d_{\text{dim}}}$ balls with radius r .*

Roughly speaking, the doubling dimension is a measure for describing the growth rate of the data set \mathcal{X} with respect to the metric $\text{dist}(\cdot, \cdot)$. As a special case, the doubling dimension of the Euclidean space \mathbb{R}^d is $\Theta(d)$.

DEFINITION B.2. (WASSERSTEIN BARYCENTER) *Given a set of probability measures \mathcal{Q} as in (2.2), the Wasserstein barycenter on \mathcal{Q} is a new probability measure $\nu^* \in \mathcal{P}(\mathcal{X})$ that minimizes the following objective*

$$WB(\mathcal{Q}, \nu) := \frac{1}{\omega(\mathcal{Q})} \sum_{l=1}^m \omega_l \cdot W_z^z(\mu^l, \nu) \text{ with } \nu \in \mathcal{P}(\mathcal{X}).$$

LEMMA B.1. *Given three points $a, b, c \in \mathcal{X}$ and a real number $z \geq 1$, the following Generalized triangle inequalities [29, 35] hold for any $0 < s \leq 1$:*

- $\text{dist}^z(a, b) \leq (1 + s)^{z-1} \text{dist}^z(a, c) + (1 + \frac{1}{s})^{z-1} \text{dist}^z(b, c)$;
- $|\text{dist}^z(a, c) - \text{dist}^z(b, c)| \leq s \cdot \text{dist}^z(a, c) + (\frac{3s}{s})^{z-1} \text{dist}^z(a, b)$.

C Proof of Section 3

Proof. (of Lemma 3.1) Equivalence of \mathcal{D}_g and \mathcal{D}_h under φ : First, we prove $\varphi : \mathcal{D}_g \rightarrow \mathcal{D}_h$ is a map. That is, given any $(\mathbf{a}_{\text{out}}^0, \mathbf{b}_{\text{out}}^0, \mathbf{P}^0) \in \mathcal{D}_g$, we need to prove $\mathbf{P}_{\text{aug}}^0 = \varphi(\mathbf{a}_{\text{out}}^0, \mathbf{b}_{\text{out}}^0, \mathbf{P}^0)$ is the only image in \mathcal{D}_h as follows. From (3.9), for any $j \in [n]$, we have

$$\sum_{i=1}^{n+1} (P_{\text{aug}}^0)_{ij} = \sum_{i=1}^n P_{ij}^0 + \frac{(b_{\text{out}}^0)_j}{1 - \zeta_\nu} = \frac{b_j^0 - (b_{\text{out}}^0)_j}{1 - \zeta_\nu} + \frac{(b_{\text{out}}^0)_j}{1 - \zeta_\nu} = \frac{b_j^0}{1 - \zeta_\nu} = (\mathbf{b}_{\text{aug}}^0)_j,$$

where the second equality comes from the fact that $(\mathbf{P}^0)^T \mathbf{1} = \frac{\mathbf{b}^0 - \mathbf{b}_{\text{out}}^0}{1 - \zeta_\nu}$ in (2.1), and the last equality is due to (3.6). Similarly, by (2.1) and (3.6), we obtain $\sum_{i=1}^{n+1} (P_{\text{aug}}^0)_{ij} = \frac{\zeta_\mu}{1 - \zeta_\mu} = (\mathbf{b}_{\text{aug}}^0)_j$ for $j = n + 1$. Till now, we have $(\mathbf{P}_{\text{aug}}^0)^T \mathbf{1} = \mathbf{b}_{\text{aug}}^0$. By a similar way, we have $\mathbf{P}_{\text{aug}}^0 \mathbf{1} = \mathbf{a}_{\text{aug}}^0$. Besides, it is obvious that $\mathbf{P}_{\text{aug}}^0 \in \mathbb{R}^{(n+1) \times (n+1)}$. Therefore, for each $(\mathbf{a}_{\text{out}}^0, \mathbf{b}_{\text{out}}^0, \mathbf{P}^0) \in \mathcal{D}_g$, we have the only $\mathbf{P}_{\text{aug}}^0 = \varphi(\mathbf{a}_{\text{out}}^0, \mathbf{b}_{\text{out}}^0, \mathbf{P}^0) \in \mathcal{D}_h$, which indicates that φ is a map. Then, it is obvious that $\varphi(\mathbf{a}_{\text{out}}^0, \mathbf{b}_{\text{out}}^0, \mathbf{P}^0) = \varphi(\mathbf{a}'_{\text{out}}, \mathbf{b}'_{\text{out}}, \mathbf{P}')$ holds only if $(\mathbf{a}_{\text{out}}^0, \mathbf{b}_{\text{out}}^0, \mathbf{P}^0) = (\mathbf{a}'_{\text{out}}, \mathbf{b}'_{\text{out}}, \mathbf{P}')$; thus, φ is an injection.

Next, to prove φ is a surjection, we construct

$$\psi : \mathcal{D}_h \rightarrow \mathcal{D}_g, \mathbf{P}_{\text{aug}}^1 \mapsto (\mathbf{a}_{\text{out}}^1, \mathbf{b}_{\text{out}}^1, \mathbf{P}^1),$$

where $P_{ij}^1 = (P_{\text{aug}}^1)_{ij}$, $(a_{\text{out}}^1)_i = (1 - \zeta_\mu) \cdot (P_{\text{aug}}^1)_{i, n+1}$, $(b_{\text{out}}^1)_j = (1 - \zeta_\nu) \cdot (P_{\text{aug}}^1)_{(n+1, j)}$ for $i, j \in [n]$. We can demonstrate that ψ is also a map by similar techniques.

Then, given any $\mathbf{P}_{\text{aug}}^1 \in \mathcal{D}_h$, we can construct $(\mathbf{a}_{\text{out}}^1, \mathbf{b}_{\text{out}}^1, \mathbf{P}^1) = \psi(\mathbf{P}_{\text{aug}}^1) \in \mathcal{D}_g$; besides, we have $\varphi(\mathbf{a}_{\text{out}}^1, \mathbf{b}_{\text{out}}^1, \mathbf{P}^1) = \mathbf{P}_{\text{aug}}^1$. That is, for any $\mathbf{P}_{\text{aug}}^1 \in \mathcal{D}_h$, we can find its preimage in \mathcal{D}_g . Thus, φ is a surjective. Therefore, φ is a bijection between \mathcal{D}_g and \mathcal{D}_h .

Equivalence of $h\varphi$ and g :

For any $(\mathbf{a}_{\text{out}}, \mathbf{b}_{\text{out}}, \mathbf{P}) \in \mathcal{D}_g$, we can construct $\mathbf{P}_{\text{aug}} = \varphi(\mathbf{a}_{\text{out}}, \mathbf{b}_{\text{out}}, \mathbf{P}) \in \mathcal{D}_h$. Then, we have

$$g(\mathbf{a}_{\text{out}}, \mathbf{b}_{\text{out}}, \mathbf{P}) = \langle \mathbf{P}, \mathbf{C} \rangle = \sum_{i=1}^n \sum_{j=1}^n P_{ij} \cdot C_{ij} = \sum_{i=1}^{n+1} \sum_{j=1}^{n+1} (P_{\text{aug}})_{ij} \cdot (C_{\text{aug}})_{ij} = \langle \mathbf{P}_{\text{aug}}, \mathbf{C}_{\text{aug}} \rangle = h(\mathbf{P}_{\text{aug}}) = h\varphi(\mathbf{a}_{\text{out}}, \mathbf{b}_{\text{out}}, \mathbf{P})$$

where the third equality comes from (3.8) and the definition of φ . Specially, from (3.8), we have $(C_{\text{aug}})_{ij} = 0$ if $i = n + 1$ or $j = n + 1$, and $(C_{\text{aug}})_{ij} = C_{ij}$ for $i, j \in [n]$; via the definition of φ , we have $P_{ij} = (P_{\text{aug}})_{ij}$ for $i, j \in [n]$. Thus, we obtain $g = h\varphi$.

Similarly, for any $\mathbf{P}_{\text{aug}} \in \mathcal{D}_h$, we can also prove $h(\mathbf{P}_{\text{aug}}) = g\varphi^{-1}(\mathbf{P}_{\text{aug}})$, where $\varphi^{-1} := \psi$. Thus, we have $h = g\varphi^{-1}$. \square

Proof. (of Theorem 3.1) For any $\mu, \nu \in \mathcal{P}(\mathcal{X})$, by combining (2.1), (3.8) and Lemma 3.1, we have $W_z^z(\mu, \nu) = \mathcal{AOT}(\mu, \nu)$. Then,

$$WB(\mathcal{Q}, \nu) = \frac{1}{\omega(\mathcal{Q})} \sum_{l=1}^m \omega_l \cdot W_z^z(\mu^l, \nu) = \frac{1}{\omega(\mathcal{Q})} \sum_{l=1}^m \omega_l \cdot \mathcal{AOT}(\mu^l, \nu) = \mathcal{AWB}(\mathcal{Q}, \nu).$$

\square

D Proof of Section 4

LEMMA D.1. *If we take a sample μ from \mathcal{Q} according to the distribution $\frac{\omega_l}{\omega(\mathcal{Q})}$, then for any $\nu \in \mathcal{P}(\mathcal{X})$ we have*

$$\mathbb{E} \left[\sum_{l=1}^m \omega_l \cdot W_z^z(\mu^l, \mu) \right] \leq 2^z \cdot \sum_{l=1}^m \omega_l \cdot W_z^z(\mu^l, \nu)$$

Proof. [of Lemma D.1] From the generalized triangle inequality in Lemma B.1, we have

$$(D.1) \quad \begin{aligned} & \mathbb{E} \left[\sum_{l=1}^m \omega_l \cdot W_z^z(\mu^l, \mu) \right] \\ & \leq \mathbb{E} \left[\sum_{l=1}^m \omega_l \cdot 2^{z-1} \cdot (W_z^z(\mu^l, \nu) + W_z^z(\mu, \nu)) \right] \end{aligned}$$

Since the expectation is taken on μ , we have

$$\begin{aligned} (D.1) &= \sum_{l=1}^m \omega_l \cdot 2^{z-1} \cdot W_z^z(\mu^l, \nu) + \sum_{l=1}^m \omega_l \cdot 2^{z-1} \cdot \mathbb{E} [W_z^z(\mu, \nu)] \\ &= \sum_{l=1}^m \omega_l \cdot 2^{z-1} \cdot W_z^z(\mu^l, \nu) + 2^{z-1} \cdot \omega(\mathcal{Q}) \cdot \mathbb{E} [W_z^z(\mu, \nu)] \\ &= 2^z \cdot \sum_{l=1}^m \omega_l \cdot W_z^z(\mu^l, \nu). \end{aligned}$$

□

Proof. (of Lemma 4.1) W.L.O.G., we assume that $\widehat{\mathcal{Q}} = \{\hat{\mu}^l\}_{l \in [m]}$ is the optimal noiseless measure set induced by the optimal solution ν^* for free-RWB on \mathcal{Q} ; that is,

$$\text{OPT} = \mathcal{WB}(\mathcal{Q}, \nu^*) = \mathcal{WB}(\widehat{\mathcal{Q}}, \nu^*) = \frac{1}{\omega(\mathcal{Q})} \cdot \sum_{l=1}^m \omega_l \cdot W_z^z(\hat{\mu}^l, \nu^*).$$

It is obvious that OPT and ν^* are also optimal value and optimal solution for Wasserstein barycenter problem on $\widehat{\mathcal{Q}}$. By combining Lemma D.1 and Markov's inequality, if we take t samples $\{\hat{\mu}^{q1}, \dots, \hat{\mu}^{qt}\}$ from $\widehat{\mathcal{Q}}$, then there exists an $2^z \alpha$ -approximate solution $\hat{\mu}$ in $\{\hat{\mu}^{q1}, \dots, \hat{\mu}^{qt}\}$ for Wasserstein barycenter problem on $\widehat{\mathcal{Q}}$ with probability at least $1 - \alpha^{-t}$.

Then, we have

$$\mathcal{WB}(\mathcal{Q}, \hat{\mu}) \leq \mathcal{WB}(\widehat{\mathcal{Q}}, \hat{\mu}) \leq 2^z \alpha \cdot \mathcal{WB}(\widehat{\mathcal{Q}}, \nu^*) = 2^z \alpha \cdot \text{OPT},$$

where the first inequality comes from that $\widehat{\mathcal{Q}}$ is the optimal noiseless measure set induced by ν^* instead of $\hat{\mu}$. ($\widehat{\mathcal{Q}}$ is the feasible noiseless measure set for $\hat{\mu}$, and is necessary the optimal one.) Thus, $\hat{\mu}$ is a $2^z \alpha$ -approximate solution for free-RWB on \mathcal{Q} .

However, $\hat{\mu}$ is unknown for us. Suppose $\widehat{\mathbf{P}}^l$ is the optimal coupling induced by Wasserstein distance between $\hat{\mu}$ and $\hat{\mu}^l$. Then, $\{\widehat{\mathbf{P}}^l\}_{l \in [m]}$ is a feasible coupling set for fixed-RWB $\mathcal{WB}_{\widehat{\mathcal{X}}}(\mathcal{Q}, \hat{\mu})$, where $\widehat{\mathcal{X}}$ is the locations of $\hat{\mu}$. Suppose $\hat{\nu} = \min_{\nu} \mathcal{WB}_{\widehat{\mathcal{X}}}(\mathcal{Q}, \nu)$, we have $\mathcal{WB}_{\widehat{\mathcal{X}}}(\mathcal{Q}, \hat{\nu}) \leq \mathcal{WB}_{\widehat{\mathcal{X}}}(\mathcal{Q}, \hat{\mu})$. For the fixed $\hat{\mu}$ and $\hat{\nu}$, their locations are both $\widehat{\mathcal{X}}$, thus $\mathcal{WB}_{\widehat{\mathcal{X}}}(\mathcal{Q}, \hat{\mu}) = \mathcal{WB}(\mathcal{Q}, \hat{\mu})$ and $\mathcal{WB}_{\widehat{\mathcal{X}}}(\mathcal{Q}, \hat{\nu}) = \mathcal{WB}(\mathcal{Q}, \hat{\nu})$.

Then, we have

$$\mathcal{WB}(\mathcal{Q}, \hat{\nu}) \leq \mathcal{WB}(\mathcal{Q}, \hat{\mu}) \leq 2^z \alpha \cdot \text{OPT},$$

which implies that $\hat{\nu}$ is a $2^z \alpha$ -approximate solution for free-RWB on \mathcal{Q} . Finally, according to the definition of $\tilde{\nu}$, $\tilde{\nu}$ must be an $2^z \alpha$ -approximate solution. □

Proof. (of Lemma 4.2) Let μ^0, μ^1 be the noiseless probability measures induced by $\mathcal{W}_z(\mu, \nu)$ and $\mathcal{W}_z(\mu, \tilde{\nu})$ respectively; that is, $\mathcal{W}_z(\mu, \nu) = W_z(\mu^0, \nu)$ and $\mathcal{W}_z(\mu, \tilde{\nu}) = W_z(\mu^1, \tilde{\nu})$. Then, we have

$$\mathcal{W}_z^z(\mu, \nu) = W_z^z(\mu^0, \nu) \leq W_z^z(\mu^1, \nu)$$

By using the generalized triangle inequality in Lemma B.1, we obtain

$$\begin{aligned} \mathcal{W}_z^z(\mu, \nu) &\leq (1+s)^{z-1} \cdot W_z^z(\mu^1, \tilde{\nu}) + (1 + \frac{1}{s})^{z-1} \cdot W_z^z(\nu, \tilde{\nu}) \\ &\leq (1+s)^{z-1} \cdot \mathcal{W}_z^z(\mu, \tilde{\nu}) + (1 + \frac{1}{s})^{z-1} \cdot r^z, \end{aligned}$$

where the last inequality comes from the definition of $\mathcal{D}_{\tilde{\nu}}$. \square

Proof. (of Lemma 4.3) According to Hoeffding's inequality, if we set $\Gamma = \frac{\log 1/\eta}{\epsilon^2}$, then the following inequality holds with probability at least $1 - \eta$ for $0 \leq k \leq K$.

$$(D.2) \quad \left| \sum_{\mu \in \mathcal{S}_k} \tau(\mu) \cdot \mathcal{W}_z^z(\mu, \nu) - \sum_{\mu \in \mathcal{Q}_k} \omega(\mu) \cdot \mathcal{W}_z^z(\mu, \nu) \right| \leq \mathcal{O}(\epsilon) \cdot \omega(\mathcal{Q}_k) \cdot (2^k H)^z$$

We set $r = H$ in Definition 2.4, then we have $W_z(\tilde{\nu}, \nu) \leq H$ for $\nu \in \mathcal{D}_{\tilde{\nu}}$. For any μ in the outermost layer \mathcal{Q}_{K+1} , by combining generalized triangle inequality and the relationship in (4.13), we have $\mathcal{W}_z^z(\mu, \nu) \in (1 + \mathcal{O}(\epsilon)) \cdot \mathcal{W}_z^z(\mu, \tilde{\nu})$ for any $\nu \in \mathcal{D}_{\tilde{\nu}}$. Then, by combining (4.15), we have (D.2) holds for $k = K + 1$.

Then, we can obtain

$$\begin{aligned} |\mathcal{WB}(\mathcal{Q}, \nu) - \mathcal{WB}(\mathcal{S}, \nu)| &= \frac{1}{\omega(\mathcal{Q})} \left| \sum_{\mu \in \mathcal{Q}} \omega(\mu) \cdot \mathcal{W}_z^z(\mu, \nu) - \sum_{\mu \in \mathcal{S}} \tau(\mu) \cdot \mathcal{W}_z^z(\mu, \nu) \right| \\ &\leq \frac{1}{\omega(\mathcal{Q})} \sum_{k=0}^{K+1} \left| \sum_{\mu \in \mathcal{Q}_k} \omega(\mu) \cdot \mathcal{W}_z^z(\mu, \nu) - \sum_{\mu \in \mathcal{S}_k} \tau(\mu) \cdot \mathcal{W}_z^z(\mu, \nu) \right| \\ &\leq \frac{\mathcal{O}(\epsilon)}{\omega(\mathcal{Q})} \cdot \sum_{k=0}^{K+1} \omega(\mathcal{Q}_k) \cdot (2^k H)^z = \mathcal{O}(\epsilon) \cdot \mathcal{WB}(\mathcal{Q}, \tilde{\nu}) \end{aligned}$$

where the first inequality follows from the partition in (4.13), the second inequality comes from (D.2), and the last inequality is due to that the partition (4.13) is anchored at $\tilde{\nu}$.

Since $\tilde{\nu}$ is an $\mathcal{O}(1)$ -approximate solution, we have $\mathcal{WB}(\mathcal{Q}, \tilde{\nu}) \leq \mathcal{O}(1) \cdot \text{OPT}$. Moreover, we know $\text{OPT} \leq \mathcal{WB}(\mathcal{Q}, \nu)$, thus $|\mathcal{WB}(\mathcal{Q}, \nu) - \mathcal{WB}(\mathcal{S}, \nu)| \leq \mathcal{O}(\epsilon) \cdot \mathcal{WB}(\mathcal{Q}, \nu)$ holds. \square

References

- [1] *Gradient-based learning applied to document recognition*, Proceedings of the IEEE, 86 (1998), pp. 2278–2324.
- [2] M. AGUEH AND G. CARLIER, *Barycenters in the wasserstein space*, SIAM Journal on Mathematical Analysis, 43 (2011), pp. 904–924.
- [3] J. M. ALTSCHULER AND E. BOIX-ADSERA, *Hardness results for multimarginal optimal transport problems*, Discrete Optimization, 42 (2021), p. 100669.
- [4] J.-D. BENAMOU, G. CARLIER, M. CUTURI, L. NENNA, AND G. PEYRÉ, *Iterative bregman projections for regularized transportation problems*, SIAM Journal on Scientific Computing, 37 (2015), pp. A1111–A1138.
- [5] V. BRAVERMAN, V. COHEN-ADDAD, H.-C. S. JIANG, R. KRAUTHGAMER, C. SCHWIEGELSHOHN, M. B. TOFTRUP, AND X. WU, *The power of uniform sampling for coresets*, in 2022 IEEE 63rd Annual Symposium on Foundations of Computer Science (FOCS), IEEE Computer Society, 2022, pp. 462–473.
- [6] V. BRAVERMAN, S. H.-C. JIANG, R. KRAUTHGAMER, AND X. WU, *Coresets for clustering in excluded-minor graphs and beyond*, in Proceedings of the 2021 ACM-SIAM Symposium on Discrete Algorithms (SODA), SIAM, 2021, pp. 2679–2696.
- [7] L. CHAPEL, M. Z. ALAYA, AND G. GASSO, *Partial optimal transport with applications on positive-unlabeled learning*, Advances in Neural Information Processing Systems, 33 (2020), pp. 2903–2913.
- [8] K. CHEN, *On coresets for k -median and k -means clustering in metric and euclidean spaces and their applications*, SIAM Journal on Computing, 39 (2009), pp. 923–947.
- [9] V. COHEN-ADDAD, D. SAULPIC, AND C. SCHWIEGELSHOHN, *Improved coresets and sublinear algorithms for power means in euclidean spaces*, Advances in Neural Information Processing Systems, 34 (2021), pp. 21085–21098.
- [10] H. DING AND M. LIU, *On geometric prototype and applications*, in 26th Annual European Symposium on Algorithms (ESA 2018), Schloss Dagstuhl-Leibniz-Zentrum fuer Informatik, 2018.
- [11] H. DING, W. LIU, AND M. YE, *A data-dependent approach for high-dimensional (robust) wasserstein alignment*, ACM Journal of Experimental Algorithmics, 28 (2023), pp. 1–32.

- [12] D. DVINSKIKH AND D. TIAPKIN, *Improved complexity bounds in wasserstein barycenter problem*, in International Conference on Artificial Intelligence and Statistics, PMLR, 2021, pp. 1738–1746.
- [13] D. FELDMAN, *Core-sets: Updated survey*, Sampling techniques for supervised or unsupervised tasks, (2020), pp. 23–44.
- [14] D. FELDMAN AND M. LANGBERG, *A unified framework for approximating and clustering data*, in Proceedings of the forty-third annual ACM symposium on Theory of computing, 2011, pp. 569–578.
- [15] S. GUMINOV, P. DVURECHENSKY, AND A. GASNIKOV, *On accelerated alternating minimization*, tech. rep., Berlin: Weierstraß-Institut für Angewandte Analysis und Stochastik, 2020.
- [16] J. HUANG, R. HUANG, W. LIU, N. FRERIS, AND H. DING, *A novel sequential coresets method for gradient descent algorithms*, in International Conference on Machine Learning, PMLR, 2021, pp. 4412–4422.
- [17] L. HUANG, S. H.-C. JIANG, J. LI, AND X. WU, *Epsilon-coresets for clustering (with outliers) in doubling metrics*, in 2018 IEEE 59th Annual Symposium on Foundations of Computer Science (FOCS), IEEE, 2018, pp. 814–825.
- [18] L. HUANG, S. H.-C. JIANG, J. LOU, AND X. WU, *Near-optimal coresets for robust clustering*, in The Eleventh International Conference on Learning Representations, 2022.
- [19] R. HUANG, J. HUANG, W. LIU, AND H. DING, *Coresets for wasserstein distributionally robust optimization problems*, Advances in Neural Information Processing Systems, 35 (2022), pp. 26375–26388.
- [20] P. HUBER, *Robust estimation of a location parameter*, Ann. Math. Statist., 35 (1964), pp. 73–101.
- [21] M. JAGGI, *Revisiting frank-wolfe: Projection-free sparse convex optimization*, in International conference on machine learning, PMLR, 2013, pp. 427–435.
- [22] A. JAMBULAPATI, A. SIDFORD, AND K. TIAN, *A direct tilde $\{O\}(1/\epsilon)$ iteration parallel algorithm for optimal transport*, Advances in Neural Information Processing Systems, 32 (2019).
- [23] N. JORGE AND J. W. STEPHEN, *Numerical optimization*, Springer, 2006.
- [24] A. KROSHNIN, N. TUPITSA, D. DVINSKIKH, P. DVURECHENSKY, A. GASNIKOV, AND C. URIBE, *On the complexity of approximating wasserstein barycenters*, in International conference on machine learning, PMLR, 2019, pp. 3530–3540.
- [25] M. LANGBERG AND L. J. SCHULMAN, *Universal ϵ -approximators for integrals*, in Proceedings of the twenty-first annual ACM-SIAM symposium on Discrete Algorithms, SIAM, 2010, pp. 598–607.
- [26] K. LE, H. NGUYEN, Q. M. NGUYEN, T. PHAM, H. BUI, AND N. HO, *On robust optimal transport: Computational complexity and barycenter computation*, Advances in Neural Information Processing Systems, 34 (2021), pp. 21947–21959.
- [27] T. LIN, N. HO, X. CHEN, M. CUTURI, AND M. JORDAN, *Fixed-support wasserstein barycenters: Computational hardness and fast algorithm*, Advances in Neural Information Processing Systems, 33 (2020), pp. 5368–5380.
- [28] S. LLOYD, *Least squares quantization in pcm*, IEEE transactions on information theory, 28 (1982), pp. 129–137.
- [29] K. MAKARYCHEV, Y. MAKARYCHEV, AND I. RAZENSHTEYN, *Performance of johnson–lindenstrauss transform for k -means and k -medians clustering*, SIAM Journal on Computing, (2022), pp. STOC19–269.
- [30] S. NARAYANAN AND J. NELSON, *Optimal terminal dimensionality reduction in euclidean space*, in Proceedings of the 51st Annual ACM SIGACT Symposium on Theory of Computing, 2019, pp. 1064–1069.
- [31] S. NIETERT, Z. GOLDFELD, AND R. CUMMINGS, *Outlier-robust optimal transport: Duality, structure, and statistical analysis*, in International Conference on Artificial Intelligence and Statistics, PMLR, 2022, pp. 11691–11719.
- [32] G. PEYRÉ, M. CUTURI, ET AL., *Computational optimal transport*, Center for Research in Economics and Statistics Working Papers, (2017).
- [33] J. RABIN, G. PEYRÉ, J. DELON, AND M. BERNOT, *Wasserstein barycenter and its application to texture mixing*, in International Conference on Scale Space and Variational Methods in Computer Vision, Springer, 2011, pp. 435–446.
- [34] D. SIMON AND A. ABERDAM, *Barycenters of natural images constrained wasserstein barycenters for image morphing*, in Proceedings of the IEEE/CVF Conference on Computer Vision and Pattern Recognition, 2020, pp. 7910–7919.
- [35] C. SOHLER AND D. P. WOODRUFF, *Strong coresets for k -median and subspace approximation: Goodbye dimension*, in 2018 IEEE 59th Annual Symposium on Foundations of Computer Science (FOCS), IEEE, 2018, pp. 802–813.
- [36] M. TUKAN, A. MAALOUF, AND D. FELDMAN, *Coresets for near-convex functions*, Advances in Neural Information Processing Systems, 33 (2020), pp. 997–1009.
- [37] D. C. VAN ESSEN, S. M. SMITH, D. M. BARCH, T. E. BEHRENS, E. YACOUB, K. UGURBIL, W.-M. H. CONSORTIUM, ET AL., *The wu-minn human connectome project: an overview*, Neuroimage, 80 (2013), pp. 62–79.
- [38] C. VILLANI ET AL., *Optimal transport: old and new*, vol. 338, Springer, 2009.
- [39] Z. WANG, Y. GUO, AND H. DING, *Robust and fully-dynamic coresets for continuous-and-bounded learning (with outliers) problems*, Advances in Neural Information Processing Systems, 34 (2021), pp. 14319–14331.
- [40] Z. WU, S. SONG, A. KHOSLA, F. YU, L. ZHANG, X. TANG, AND J. XIAO, *3d shapenets: A deep representation for volumetric shapes*, in Proceedings of the IEEE conference on computer vision and pattern recognition, 2015, pp. 1912–1920.